Università degli Studi di Ferrara

DOTTORATO DI RICERCA IN
FISICA

CICLO XXI

COORDINATORE Prof. Filippo Frontera

Spin-dependent scattering of the conduction electrons in nanogranular Fe-Ag films

Settore Scientifico Disciplinare Fis/01

Dottorando
Dott. Melissa Tamisari

Tutore
Prof. Franco Ronconi

Anni 2006/2008

A mio nonno

Contents

Chapter 1

Introduction

The magnetoresistance (MR), the change of resistance of a conductor when it is placed in an external magnetic field, is a research argument from a lot of time, both for the information of structural character and compositional deduced from it, but also thanks to the possibility to use such effect for the preparation of sensors of magnetic field. The MR effect has been of substantial importance technologically, especially in connection with read-out heads for magnetic disks and sensors of magnetic fields. Applications of this type have also been favourite from the recent discovery of a new phenomenon that allows to produce devices displaying a great versatility and that allow to get notable variations of resistance in correspondence with small applied magnetic fields. Thanks to this last characteristic the effect has been suitable with the term *giant magnetoresistance* (GMR). The use of "*giant*" refer not only to point out the entity of the observed effect but also to differentiate it from similar phenomena that, also producing resistivity variations in a material, have a different origin. In fact, otherwise from the ordinary and anisotropy magnetoresistance, rising from the Lorentz force and from the spin-orbit coupling, respectively, the origin of GMR is a scattering of the conduction electrons which cross section is a function of the electronic spin. To have scattering of the conduction electrons is necessary the contact

between materials with two different band structure. The first observation of GMR was made in magnetic multilayer, where layers of ferromagnetic and non-magnetic metals are stacked on each other. The widths of the individual layers are of nanometre size. Subsequently the GMR was observed in granular magnetic materials, composed of nanosized superparamagnetic clusters embedded in a non-magnetic matrix.

The activity of this Ph-D has been devoted to the growth and the characterization of granular thin film of Fe-Ag. The materials used for the preparation are iron and silver because the two metals are immiscible and the GMR effect associated to this couple of metals it is usually very elevated. The deposition technique used to make the films is a particular methodology that does not create an alloy, a low efficacy system for GMR observation, but allows a fine dispersion of magnetic particles in the non magnetic matrix. The research regards the magnetic and magnetoresistive properties of the nanogranular films, comparing the results with structural investigation, to understand the best system structure (Fe concentration and structural arrangement) that produces the maximum GMR effect and the maximum efficiency.

In the first part, an introduction about the transport properties of magnetic nanostructures and the origin of the giant magnetoresistive effect in multilayer and nanogranular films is reported. Afterwards a description of the magnetic properties of the magnetic nanocluster is presented.

In the second part, a description of a few experimental apparatuses for samples preparation and characterization is presented. Great attention is devoted to the description of the deposition technique used to make the films because it is a particular methodology that allows the thin film deposition out of the thermodynamic equilibrium.

The third part is devoted to the analysis and the discussion of the experimental results. The magnetic and magnetoresistive measurements are correlated with the structural investigation to understand the best arrangement to obtain the maximum of GMR efficiency.

Chapter 2

Giant Magnetoresistance effect: basics of theory

Giant magnetoresistance (GMR) is one of the most fascinating discoveries in thin-film magnetism, which combines both technological potential and deep fundamental physics, Nobel Prize in Physics in 2007 to Albert Fert and Peter Grünberg. In 1988, Baibich et al. discovered giant magnetoresistance in Fe/Cr multilayers. Like other magnetoresistive effects, GMR is the change in electrical resistance in response to an applied magnetic field. Baibich's group discovered that the application of a magnetic field to a Fe/Cr multilayer resulted in a significant reduction of the electrical resistance of the multilayer. This effect was found to be much larger than either ordinary or anisotropic magnetoresistance and was, therefore, called "giant magnetoresistance" or GMR. A similar, though diminished effect was discovered in Fe/Cr/Fe trilayers [1]. Since the discovery of GMR a large number of magnetic multilayer structures, which display the GMR effect with very different intensity, have been discovered. It was found that the magnitude of GMR varies considerably depending on the chemical constituents of the multilayer. GMR to a great extent is determined by the ferromagnetic metal/nonmagnetic metal

pair, rather than by an individual material considered separately. For example, GMR was found to be much lower in Co/Cr and Fe/Cu multilayers (3% in Co/Cr4 and 5.5% in Fe/Cu57), as compared to the Fe/Cr and Co/Cu multilayers [2, 3]. The use of "giant" refers to the origin of the MR effect; it does not always refer to the magnitude of the effect. This effect can be distinguished from the ordinary MR coming from the direct action of the magnetic field on the electron trajectories, the Lorentz force; and from the anisotropic MR which comes from dependence of the resistivity on the relative orientation of the magnetization to the current. The typical structure is ferromagnetic layers alternate with non-magnetic layers. The role of the external magnetic field is to change the internal magnetic configuration; in cases where this is not possible, e.g., if the layers are coupled ferromagnetically, or so strongly antiferromagnetically coupled that ordinary fields cannot rotate one layer relative to another, giant MR does not appear. For this reason, ordinary magnetic metals do not display this MR effect, and it is necessary to separate the magnetic regions from one another so as to be able to reorient their magnetizations. Magnetic layers with nonmagnetic spacer layers was the first structure to produce this result. More recently, precipitating out magnetic granules in a nonmagnetic metallic matrix also produces the physical separation of the magnetic entities.

In this chapter a wide introduction to GMR effect phenomenology in magnetic multilayers and nanogranular systems is reported. The main aspects of the transport properties of magnetic nanostructures, and the magnetic properties of magnetic nanocluster are summarized. The purpose is to introduce the different fields with which this work is concerned and review the concepts and the formalism that will be useful for further discussion.

2.1 Electron scattering at the ferromagnetic/ diamagnetic interface

In the free atoms, the $3d$ and $4s$ atomic energy levels of the $3d$ transition elements are hosts for the valence electrons. In the metallic state these $3d$ and $4s$ levels are broadened into energy bands. Since the $4s$ orbitals are rather extended in space there will be a considerable overlap between $4s$ orbitals belonging to neighbouring atoms, and therefore the corresponding $4s$ band is spread out over a wide energy range (15−20 eV). In contrast to this, the $3d$ orbitals are much less extended in space. Therefore the energy width of the associated $3d$ energy band is comparatively narrow (4−7 eV). In practice one cannot make a clear distinction between the $3d$ and $4s$ orbitals since they will hybridize strongly with each other in the solid. Nevertheless for simplicity this two band picture will be used here and the $3d$ electrons will be considered as metallic - i.e. they are itinerant electrons and can carry current through the system, although they are still much less mobile than the $4s$ electrons. A useful concept in the theory of solids is the electron density of states (DOS), $n(E)$, which represents the number of electrons in the system having energy within the interval $(E, E + dE)$. According to the exclusion principle for fermions (in this case electrons), only one electron can occupy a specific state. However each state is degenerate with respect to spin and can therefore host both an electron with spin up and an electron with spin down. In the ground state all the lowest energy levels are filled by electrons and the highest occupied energy level is called the Fermi energy, E_F.

In figure 2.1a the density of states is illustrated schematically for a non-magnetic $3d$ metal, sometimes referred to as a paramagnet, where there are equally many electrons with spin up as with spin down, i.e. there is no net magnetization. The so called spin polarization, P,

$$P = (N\uparrow - N\downarrow)/(N\uparrow + N\downarrow)$$

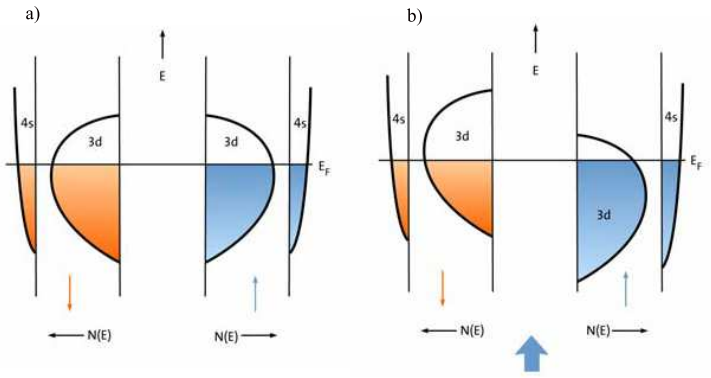

Figure 2.1: In the plot a is shown for the energy band structure of a d transition metal. The density of states $N(E)$ is shown separately for the spin up and down electrons and where a simplified separation has been made between the $4s$ and $3d$ band energies. For the non-magnetic state these are identical for the two spins (figure a). All energy levels below the Fermi energy are occupied states. The coloured area corresponds to the total number of valence electrons in the metal. In the picture b is illustrated for a ferromagnetic state, with a spin-polarization chosen to be in the up direction ($N\uparrow > N\downarrow$). This polarization is indicated by the thick arrow at the bottom of the figure b.

where $N\uparrow$ ($N\downarrow$) = number of electrons with spin up (down), is here equal to zero. For a ferromagnet ($N\uparrow$ (majority-spin electrons) is larger than $N\downarrow$ (minority-spin electrons), so that there is a net spin polarization, $P > 0$. In order to compare the energy for the ferromagnetic state with the energy for the paramagnetic state one can start from the paramagnetic state and allow for a small imbalance in the number of spin up and spin down electrons. A transfer of spin down electrons from the spin down band into the spin up band leads to more exchange energy in the system, which means a lowering of the total energy (a gain). On the other hand such a process requires a

transfer of electrons from spin down levels below the initial Fermi energy, into spin up levels situated just above the initial Fermi energy. This will necessarily lead to a loss of band energy, "kinetic energy" and thus to an increase of the total energy (a loss). Thus there is a competition between two opposite effects. This can be formulated as the so called Stoner criterion [4] for magnetism, namely that when $JN(E_F) > 1$, the system will be a ferromagnet. Here J is called the Stoner exchange parameter and $N(E_F)$ is the density of states at the Fermi energy. The Stoner parameter has a specific value for the individual element, while $N(E_F)$ depends much more on the particular spatial arrangements of the atoms relative to each other (like crystal structure). Furthermore, $N(E_F)$ tends to be high for systems with narrow energy bands as is the case for the heavier $3d$ transition elements (Fe, Co and Ni). This is the explanation for the ferromagnetism among the d transition metals. The Stoner criterion is satisfied for bcc Fe, fcc Co and fcc Ni. Due to the exchange splitting of the d bands, the number of occupied states is different for the spin up and spin down electrons, giving rise to the non-zero magnetic moments of 2.2 μ_B, 1.7 μ_B and 0.6 μ_B for Fe, Co and Ni respectively. The situation for a ferromagnet spin polarization is illustrated in figure 2.1b (with a direction chosen to be upwards). The vertical displacement between the spin up and spin down densities of states exemplifies the exchange energy splitting between the spin up and spin down energy bands, which is relevant for the metals Fe, Co and Ni. In particular the density of states at the Fermi energy $N(E_F)$ can now be very different for the two spin bands. This also means that for a ferromagnet the character of the state at the Fermi energy is quite different for spin up and spin down electrons. This is an important observation in connection with the GMR effect. The conductivity is determined by the position of the Fermi energy with respect to the d bands. In the case of Ag, diamagnetic metal, the d bands are fully occupied and the Fermi level lies within the sp band. Due

to the high velocity of the electrons within the sp band and the low density of states with resultant low probability of scattering, the mean free path is long and Ag is a very good conductor. This is also the case for the other metals like Cu and Au. On the other hand, in the case of a ferromagnetic metal like Fe, as a result of the exchange splitting, the majority d band is fully occupied, whereas the d minority band is only partly occupied. The Fermi level lies, therefore, within the sp band for the majority spins but within the d band for the minority spins. The exchange splitting of the spin bands leads to a crucial difference in the conductivity between the majority- and minority-spin electrons. The two adjacent metals, one ferromagnetic (FM) and one non-magnetic (NM) creating the interface have different band structures, which lead to a potential step at the interface. If the interface separates ferromagnetic and non-magnetic metals the transmission will be spin-dependent due to the spin dependence of the band structure of the ferromagnetic layer. If the band structure of FM is similar to the band structure of the majority spins NM, there is a good band matching that implies a high transmission for the majority-spin electrons across the FM/NM interface. On the contrary, there is a relatively large band mismatch between NM and the minority spins in FM and consequently the transmission of the minority-spin electrons across the FM/NM interface is expected to be poor. Therefore, the interfaces of the FM/NM multilayer act as spin-filters. When the filters are aligned, the majority spin-electrons can pass through relatively easily. When the filters are antialigned, the electrons in both spin channels are reflected at one of the interfaces. This spin-dependent transmission is an important ingredient of the electronic transport in GMR structures. Band matching also plays an important role in the spin-dependent interface scattering due to the intermixing of atoms near the interfaces. If we ignore the change in the chemical state of the atoms, i.e. assume that their atomic energy levels and magnetic moments are identical to those in the bulk of the adjacent layers,

then the intermixing at the interface produces a random potential which is strongly spin-dependent. This spin dependence is a direct consequence of the good band matching for the majority spins in FM/NM, which implies a small scattering potential, and the poor band matching for the minority spins in FM/NM, which implies a large scattering potential. A similar behaviour takes place in Fe/Cr multilayers [2], where a very small scattering potential (good band matching) is expected for the minority-spin electrons, but a large scattering potential (bad band matching) is expected for the majority-spin electrons. Thus, the matching or mismatching of the bands between the ferromagnetic and nonmagnetic metals results in spin-dependent scattering potentials at disordered interfaces, which can contribute to GMR.

2.2 Origin of Giant Magnetoresistance in magnetic multilayers

The GMR-effect arises as a result of spin-dependent scattering at the interfaces between ferromagnetic and non magnetic layers. As proposed first by Mott [5, 6], the conductance of ferromagnetic materials can be viewed as the sum of separate contributions from electrons with opposite spin directions when the spin quantum number of the conduction electrons is conserved in the most of the scattering processes. This so-called two-current model is a fair approximation for ferromagnets based on Fe, Co and Ni, at least at temperatures well below the Curie temperature.

Using Mott's arguments it is straightforward to explain GMR in magnetic multilayers. We consider collinear magnetic configurations, as is shown in figure 2.2, and assume that the scattering is strong for spin-down electrons and is weak for spin-up electrons. This is supposed to reflect the asymmetry in the density of states at the Fermi level, in accordance with Mott's second argument. For the parallel aligned magnetic layers (fig. 2.2a), the up-

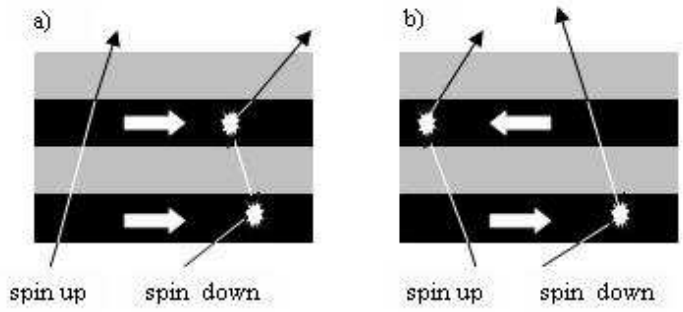

Figure 2.2: Schematic illustration of electron transport in a multilayer for parallel (a) and antiparallel (b) magnetizations of the successive ferromagnetic layers. The magnetization directions are indicated by the arrows. The solid lines are individual electron trajectories within the two spin channels.

spin electrons pass through the structure almost without scattering, because their spin is parallel to the magnetization of the layers. On the contrary, the down-spin electrons are scattered strongly within both ferromagnetic layers, because their spin is antiparallel to the magnetization of the layers. Since conduction occurs in parallel for the two spin channels, the total resistivity of the multilayer is determined mainly by the highly-conductive up-spin electrons and appears to be low. For the antiparallel-aligned multilayer (fig. 2.2b), both the up-spin and down-spin electrons are scattered strongly within one of the ferromagnetic layers, because within the one of the layers the spin is antiparallel to the magnetization direction. Therefore, in this case the total resistivity of the multilayer is high.

The combined effects of this spin-dependent scattering result in the spin filtering of the electron current when it passes through a ferromagnetic material, with the minority electrons usually experiencing more scattering. A GMR material exploits this spin-dependent scattering in a specially designed and fabricated structure. The simplest, a magnetic bilayer structure, can be modelled using a resistor network (figure 2.3 and equation (1)) in which the

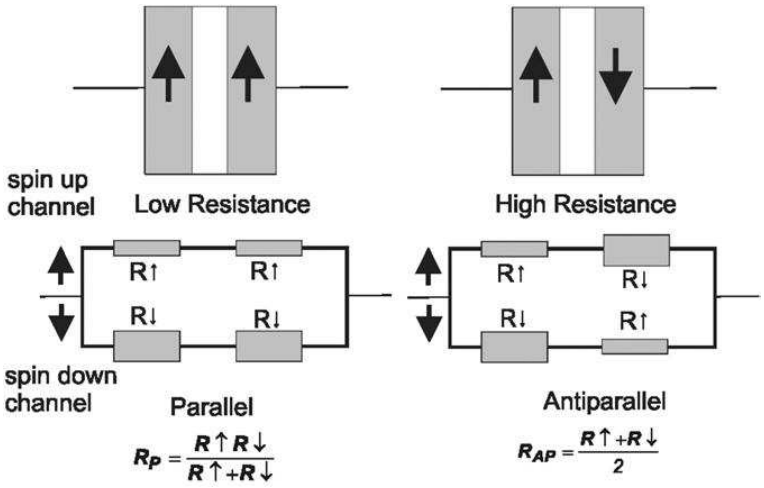

Figure 2.3: A schematic representation of GMR using a simple resistor network model. In the picture a, the spin-up channel is the majority spin channel in both the ferromagnetic layers, experiencing a low resistance ($R\uparrow$) throughout the structure. In the picture b the spin-up channel is the majority spin channel ($R\uparrow$) in the first magnetic layer but the minority-spin channel ($R\downarrow$) in the second magnetic layer and vice versa for the spin-down channel. Neither spin channel is of low resistance throughout the structure and the overall resistance state of the structure is high. GMR occurs when the relative orientation of the magnetic layers is switched, usually by the application of a magnetic field.

independent spin-up and spin-down electron current channels are represented by two parallel circuits and the resistance of the different layers represented by resistors:

$$\frac{\Delta R}{R} = \frac{R_{AP} - R_P}{R_P} = \frac{(R\downarrow - R\uparrow)^2}{4R\downarrow R\uparrow}$$

In the first case, the magnetic layers are aligned parallel and the two spin channels experience quite different resistance. One of the electron channels will be the minority electron channel, experiencing significant scattering in both the layers, whereas the other channel will be majority electrons in both

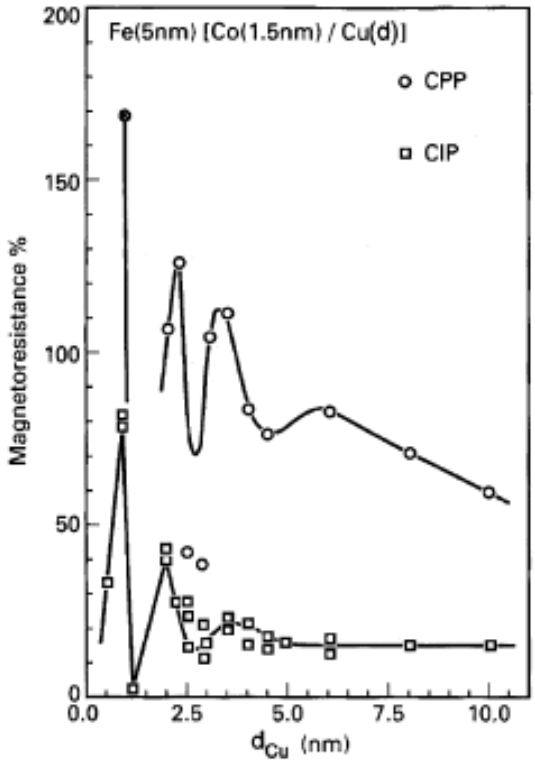

Figure 2.4: Variation of the CPP and CIP GMR as a function of the non-magnetic Cu thickness [7].

layers and will be much less scattered. Consequently the majority electron channel will dominate the conductivity in the parallel circuit and the combined structure will have a low total resistance. Conversely, in the second case, where the magnetic layers are antiparallel, both spin channels will in turn become majority or minority electrons as they travel through the different layers. Neither spin channel can therefore provide a low resistance path through the circuit and the combined resistance of the structure is consequently higher. GMR occurs when a magnetic structure is created which can be switched between the antiparallel and parallel alignment, thereby switching from a high to a low resistance state. GMR effects have been obtained in

different geometries. In the first one the current and the magnetic field can be assumed to be uniform in the direction of the transport which is the plane of the layers (CIP), while in the second one the current flows perpendicular to the plane of the layers (CPP). As in the CIP geometry, the dependence of the GMR ratio on the nonmagnetic thickness exhibits an oscillatory behaviour as shown in figure 2.4. From this figure, it turns out that the CPP-GMR is definitely larger than the CIP-GMR and exists at much larger thicknesses. These differences are due to the two different scaling lengths of the problem. Whereas the scaling length of the CIP geometry is the mean free path λ, due to spin accumulation effects, the scaling length of the CPP geometry is the spin diffusion length, l_{sf} ; which is ten times larger than the mean free path. According to Mott's first argument, the conductivity of a metal is the sum of the independent conductivities for the up-spin and down-spin electrons:

$$\sigma = \sigma_{\uparrow} + \sigma_{\downarrow}$$

Within each conduction channel the conductivity is determined by various factors. In order to illustrate their role we use the Drude formula [8] which can be expressed as follows:

$$\sigma_{Drude} = \frac{e^2}{\pi\hbar}\frac{k_F^2}{6\pi}\lambda$$

Here σ_{Drude} is the Drude conductivity per spin, $e^2/\pi\hbar \approx 0.38710^{-4}\Omega^{-1}$ is the spin conductance quantum, k_F is the Fermi momentum, and λ is the mean free path, which is the product of the relaxation time τ and the Fermi velocity v_F, $\lambda = v_F\tau$. The conductivity is determined by the electrons which have the Fermi energy. Due to the Pauli exclusion principle the electrons which lie below the Fermi level can not gain energy responding to the small applied electric field, because all the states at higher energies are occupied. As a consequence, only electrons at the Fermi level can contribute to the electric current. As can be seen from Eq.(1.2), the conductivity is proportional to

the cross sectional area of the Fermi surface, which characterizes the number of electrons contributing to the conduction. The mean free path depends of the Fermi velocity and the relaxation time, the latter can be estimated from the Fermi golden rule

$$\tau^{-1} = \frac{2\pi}{\hbar} \langle V_{scat}^2 \rangle \, n(E_F)$$

Here $\langle V_{scat}^2 \rangle$ is an average value of the scattering potential and $n(E_F)$ is the density of electronic states at the Fermi energy E_F for the appropriate spin. Although all the quantities which enter in the last expressions are in general spin-dependent, the origin of the spin dependence is different. The Fermi momentum k_F and the Fermi velocity v_F are intrinsic properties of the metal and entirely determined by the electronic band structure of the metal. In ferromagnetic metals these quantities are different for the up- and down-spin electrons. The density of states at the Fermi energy $n(E_F)$ is also determined by the spin-polarized band structure. It is the density of states, which was referred to by Mott, arguing that the scattering rates in ferromagnetic metals are spin-dependent. On the contrary, the scattering potential $\langle V_{scat}^2 \rangle$ is not an intrinsic property of the metal. It is generated by the scatterers such as defects, impurities, or lattice vibrations. The scattering potential can be either spin-dependent or spin-independent, which is determined by the particular mechanism of scattering.

Next important concept is to determine how long these electrons retain their spin orientation. It is important to calculate how large is this spin diffusion length, l_{sd} and on what parameters it depends. Considering a newly injected up-spin arriving across the interface into the nonmagnetic material, undergoes a number N of momentum changing collisions before being flipped (on average after time $\tau_{\uparrow\downarrow}$). The average distance between momentum scattering collisions is λ, the mean free path. We can now make two relations we can say that the average distance which the spin penetrates into the nonmagnetic material (perpendicular to the interface) is $\lambda\sqrt{\frac{N}{3}}$. This distance is

l_{sd}, the spin diffusion length which we wish to estimate. Moreover, the total distance walked by the spin is Nλ which, in turn, equals its velocity (the Fermi velocity, v_F) times the spin-flip time $\tau_{\uparrow\downarrow}$. Eliminating the number N of collisions gives

$$l_{sd} = \sqrt{v_F \ \tau_{\uparrow\downarrow} \ \lambda/3}$$

A rigorous analysis of the spin-accumulation length in terms of the respective electrochemical potential of the spin channels follows the model of Valet and Fert [9].

Now that we have considered the basic principles behind the origin of spin asymmetry, we can consider an important phenomenon which lies at the heart of early spin electronic devices. Providing one carrier spin type is dominant in the electrical transport of a ferromagnet, when a current is passed from this ferromagnet to a NM metal, it brings with it a net injection of spin angular momentum and hence also of magnetization [10]. The magnetization which builds up in the new material is known as a spin accumulation. Its size is determined by the equilibrium between the net spin-injection rate at the interface and the spin-flipping rate in the body of the paramagnet. It follows that the spin accumulation decays exponentially away from the interface on a length scale called the "spin diffusion length".

When spin polarized current is driven from a ferromagnetic film into a nonmagnetic film faster than the spin polarization can diffuse away from the interface, a nonequilibrium population of spin-palarized electrons builds up in a region of thickness L_s. This nonequilibrium magnetization is described as inequivalent chemical potentials for the spin-up and spin-down subbands of the normal metal. Because spin and charge are both carried by the electron, a gradient od spin density results in an electric field, which can generate current flow or produce differences in voltage. The magnitude of spin accumulation can be given in terms of the spin density n at distance x from the interface

and is

$$n = n_0 \exp \frac{-x}{l_{sd}}$$

Integrating,

$$\int_0^\infty n dx = n_0 l_{sd}$$

is the total number of spins in the accumulation and the spin decay rate

$$\frac{n_0 l_{sd}}{\tau_{\uparrow\downarrow}} = \frac{n_0 \lambda v_F}{l_{sd}}$$

must be equal to the injected spin current PJ/q where P is the polarization of the ferromagnet, J is total electrical current, q is electronic charge, λ is mean free path, v_F is Fermi velocity and n_0, the density at the interface, is given by

$$n_0 = \frac{3PJl_{sd}}{qv_F\lambda}$$

The value of GMR decreases monotonically with increasing non-magnetic layer thickness. This decrease can be qualitatively ascribed to two factors. (i) With increasing spacer thickness the probability of scattering increases as the conduction electrons traverse the spacer layer, which reduces the flow of electrons between the ferromagnetic layers and consequently reduces GMR. (ii) The increasing thickness of the nonmagnetic layer enhances the shunting current within the spacer, which also reduces GMR.

2.3 The GMR effect in magnetic nanogranular systems

Provided the basic criteria for GMR are satisfied, the layering of the different materials is not required. This was first demonstrated in 1992 by Berkowitz et al [11] and Xiao et al [12] both of whom created GMR single film materials from heterogeneous alloys in which single domain ferromagnetic particles are embedded in a non-magnetic matrix. The attraction of

these materials is that they can be very easily manufactured, provided the ferromagnetic and non-magnetic materials are immiscible, using techniques such as co-deposition or even mechanical alloying to produce a bulk material with a nanoscale microstructure. Granular materials are like the multilayers CPP configuration even if the system is not periodic like multilayers. In fact, the ideal sample has ferromagnetic regions, with the same dimensions and with the same distance between them, embedded in non-magnetic matrix. So λ is the only important parameter to have GMR effect.

The GMR effect in granular metals is attributed to the spin-dependent scattering at the interface between the magnetic particles and the matrix. It occurs when the size of the particles is comparable to the electronic mean free path (few nanometres). Due to their small size, which does not exceed the correlation length for the exchange interactions, the particles consist of a single magnetic domain. When the thermal energy exceeds the magnetic anisotropy barrier the particles become superparamagnetic and in the absence of external field their magnetization vectors point in random directions. In the random configuration the system has the maximum resistivity. Application of a magnetic field aligns the magnetic moments and the resistivity of the sample drops leading to the GMR effect. The scattering potential experienced by the conduction electrons in dilute magnetic alloys is of the following form:

$$H = V(\mathbf{r}) - 2J(\mathbf{r})\mathbf{s} \cdot \mathbf{S}$$

where $V(\mathbf{r})$ describes the spin-indipendent interaction and the $J(\mathbf{r})$ the exchange interaction between the electrons with spin $\mathbf{s}$ and the magnetic scatterers with spin $\mathbf{S}$. It describe the GMR in magnetic multilayers but it is applicable to magnetic granular solids after some modifications. Because the finite size of the magnetic particles, the effective spin **S'** affecting the conduction electrons is only a portion of the total spin $\mathbf{S}$ of the magnetic particle. If surface scattering is dominant, then **S'** will be mostly confined

on the surface. To evaluate the spin-dependent scattering in granular system, it used the first-order Born approximation and neglect the effects of multiple scattering. In these hypothesis the resistivity in granular systems [13] is:

$$\rho = \rho_d \left[1 - \frac{B^2 M^2}{M_S^2}\right] + \rho_0$$

where ρ_d is the resistivity caused by magnetic scattering and ρ_d is the partial resistivity caused by nonmagnetic mechanism, e.g. disorders and phonons. The common parameter in litterature to quantify the resistivity variation is:

$$\frac{\Delta\rho}{\rho} = \frac{\rho(H_{max}) - \rho(H=0)}{\rho(H=0)}.$$

Replacing the ρ value in the last expression:

$$\frac{\Delta\rho}{\rho} = \frac{B^2 M^2}{M_s^2(1+\rho_d/\rho_0)} = \gamma \left(\frac{M}{M_s}\right)^2$$

where γ is a global indication of how effective is the granular structure in producing GMR (GMR efficiency).

2.3.1 Superparamagnetism of fine particles

To have GMR effect the ideal structure is fine magnetic particles embedded in a non magnetic matrix. Fine magnetic particles have a superparamagnetic behaviour. Superparamagnetism is a phenomenon by which magnetic materials may exhibit a behavior similar to paramagnetism at temperatures below the Curie or the *Néel* temperature. Superparamagnets consist of individual magnetic domains of elements that have ferromagnetic properties in bulk. Theoretical predictions concerning energetic stability of a single magnetic domain were established by Kittel [14], defining a certain critical size of a particle (typically nanometers for usual ferromagnets); in smaller particles formation of a single ferromagnetic domain is preferred. Moreover, it was shown by *Néel*, that at temperatures above the so-called blocking temperature T_B, a stable bulk magnetization cannot be established due to

thermal fluctuations acting on small particles and consequently the system exhibits superparamagnetism (SPM) [15]. At low temperatures (below T_B) the thermal fluctuations do not dominate and magnetic moments of SPM particles 'freeze' in random orientation and cannot rotate freely. Already the first model of magnetization reversal in a single-domain particle (assuming coherent rotation of the magnetic domain moment) presented by Stoner and Wohlfarth [16] suggested existence of high coercivity fields below T_B, when the energy of magnetocrystalline anisotropy becomes comparable with the thermal activation energy. At temperatures above T_B (supposing a system of uniform non-interacting nanoparticles) the thermal effects allow flips of magnetic moments between the easy magnetization directions by getting over the energy barriers in zero field and consequently the $H_C = 0$. At temperatures ($T < T_B$) the thermal activation cannot overcome the magnetocrystalline anisotropy and the magnetic moment of each particle rotates from the field direction back to the nearest easy magnetization axis that yields a non-zero coercivity field. Since the nanoparticles and so the corresponding easy magnetization directions are randomly oriented, the total magnetization is naturally reduced with increasing temperature.

In a cluster every atom has a magnetic moment of the order of μ_B and all atomic moments are aligned, giving rise to a total magnetic moment $\vec{\mu}$. Because of quantization, the projection of $\vec{\mu}$ along a fixed arbitrary direction, can assume only discrete values but, if μ is sufficiently big, these values can be considered continuous and a semiclassical treatment is justified. The cluster magnetic moment can, in this approximation, point in any direction of space. Let us now consider an ensamble of identical particles; the total magnetization of the system, $\vec{M}$, is given by the vectorial sum of all single magnetic moments. As it happens for the atomic magnetic moments in a paramagnet, the average magnetization will be zero in the absence of magnetic field since all magnetic moments are randomly directed in space. When

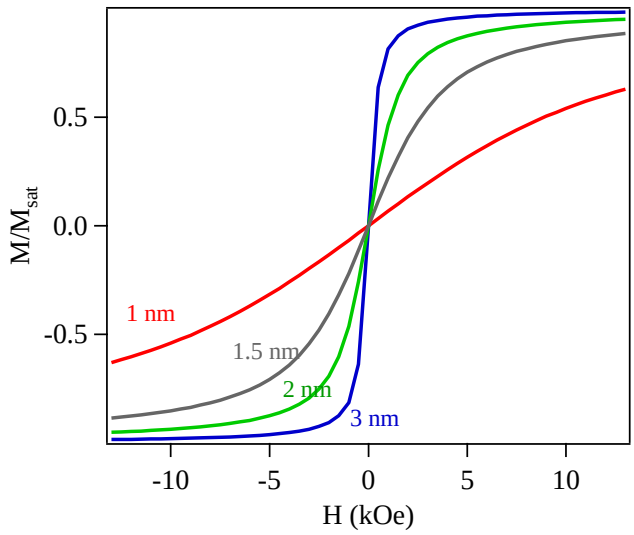

Figure 2.5: The ideal trend of magnetization in function of magnetic field for superparamagnetic particles with different dimension.

a magnetic field $\vec{H}$ is applied, they will orient and give rise to a net magnetization. The Hamiltonian of a single macrospin can then be written as: $\mathcal{H} = -\mu H \cos\theta$, where θ is the angle between the magnetic moment and the axis of the magnetic field, that is assumed to be z. The total magnetization can be found averaging over the ensamble:

$$\frac{\langle M_z \rangle}{M_s} = \coth\left(\frac{\mu H}{k_B T}\right) - \frac{\mu H}{k_B T} = \mathcal{L}\left(\frac{\mu H}{k_B T}\right)$$

where $\mathcal{L}(y) = \coth(y) - \frac{1}{y}$ is the $Langevin function$ and has the form shown in figure 2.5. From the last expression it can be remarked that the magnetic behaviour of a superparamagnetic system is determined by the competing actions of the external field and of thermal agitation. As a consequence, magnetization scales as H/T. Until now it was assumed that the macrospin is free to rotate in all directions of space. This is actually not true if the anisotropy energy is taken into account since in this case the coupling with the crystalline structure will force the magnetic moment to align in a preferential direction. For an easy comprehension let us consider the simplest scenario in

which clusters have one easy axis that induces a double well potential, with an energy barrier defined by the anisotropy: $\Delta E = K_a V$, where V is the volume of the particle. Depending on the temperature, two different regimes will then be observed: if $k_B T \gg K_a V$ energy barrier can be easily overcome and a superparamagnetic behaviour is observed; if $k_B T \ll K_a V$ the magnetic moment is strongly coupled to the crystalline structure and the particle is said to be blocked. In the range of temperature in which the two energies are of comparable magnitude, a fluctuation of the macrospin is observed with a characteristic time:

$$\tau = \tau_0 \exp\left(\frac{K_a V}{k_B T}\right)$$

where τ_0 is related to the natural frequency of gyromagnetic precession and lies in the range $10^9 - 10^{13} Hz$. A consequence of these fluctuations is that the system will appear blocked or superparamagnetic depending on the characteristic observation time: the blocking temperature (T_B) below which the moment is coupled to the lattice is not unequivocally determined, but depends on the analysis technique used to make the measurement. If the magnetic particles are kept well separated one from the other, they can be considered as independent and the only forces they will experience are due to the external magnetic field and temperature (supposing the particles isotropic). Under the additional hypothesis that particles are sufficiently small to be considered as monodomain, the system can be treated like superparamagnetic particles and the magnetization follows a Langevin curve [17].

The increase of the apparent macrospin with temperature obviously does not reflect a real increment of the magnetic moment per cluster but it is rather an indication that interactions occur between particles: when concentration is increased, the inter-particle distance becomes sufficiently low to allow dipole-dipole interactions to take place. These interactions act as a random field that opposes to the external field and hinders the moments to align. Since this effect is competing with the external field as temperature does, one can

attempt to take account of it in the superparamagnet model, introducing a temperature correction to the Langevin function. The reason why the correction term is added to the temperature rather than to the field, is that its effect does not give any contribution to the ordering of macrospins, but goes rather in the opposite direction and enhances the disorder

The magnetic behaviour of an assembly of possibly interacting single-domain superparamagnetic particles presented by Allia and co-workers [18]:

$$M(H) = M_S \int f(V)\mathcal{L}(\mu(V)(H \pm H_{eff}dip(H))/k_BT)dV$$

where $\mathcal{L}(x)$ is a Langevin function, M_S is the saturation magnetization, $\mu(V)$ is the magnetic moment of a grain having volume V, $f(V)$ is the lognormal distribution of particles sizes, and the term $H_{eff}dip(H)$ represents the contribution of dipolar interactions.

Considering the formulas of GMR showed in the previous paragraph, $\Delta\rho/\rho$ in a system of superaparamagnetic particles embedded in a non-magnetic matrix is:

$$\frac{\Delta\rho}{\rho} = \frac{B^2M^2}{M_s^2(1+\rho_d/\rho_0)} = \gamma\left(\frac{M}{M_s}\right)^2$$

A typical trend of $\Delta\rho/\rho$ in function of magnetic field is presented in figure 2.6.

The dependence of $\Delta\rho/\rho$ on M is quadratic [12]. This dependence of the GMR on the square of the total magnetization is an indication that long range correlations between the particle moments determine the size of the effect. However, many experimental groups have observed deviations from the linear dependence that have been attributed to interparticle interactions [19], to particle size distribution [12, 20], and to the coexistence of blocked and superparamagnetic particles [21] or collectively rotating and superparamagnetic particles [22] in the sample. For superparamagnetic systems, the parabolic dependence of the GMR on the total magnetization [23, 24] was proved. Zhang and Levy [23] assumed further that a distribution of the

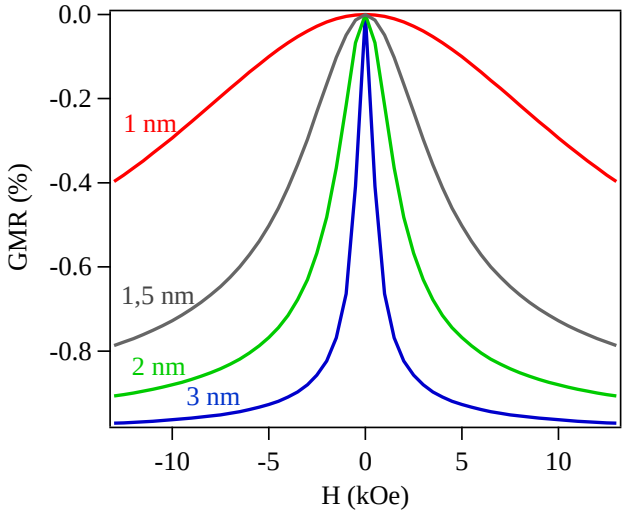

Figure 2.6: The ideal trend of $\Delta\rho/\rho$ in function of magnetic field for a system with particles with different dimension.

particle sizes exists and they showed that this is responsible for the deviations from the parabolic dependence at high fields ($M/M_s \sim 1$) in agreement with Xiao et al. experiments [12]. The situation with the deviations at low fields ($M/M_s \sim 0$) appears more complicated. The reason being that both grain-size distribution and interparticle interactions are responsible for these deviations [20].

The presence of interparticle interactions gives rise to correlations between the directions of the grains magnetic moments [25] and this has a twofold effect on GMR. On the one side, these correlations introduce locally a higher degree of order in the zero-field magnetic configuration with respect to the noninteracting case. Since the total resistivity change relies on the degree of order induced by an external magnetic field [23]; in this case the effect of the field is reduced and GMR intensity is decreased. On the other, interparticle interactions influence also the dynamic properties of the system and this affects the dependence of GMR on external magnetic field.

Experiments have revealed various factors that determine the magnitude

of the GMR effect. In particular, the value of GMR increases initially with increasing grain diameter and it decreases above a certain grain size. The maximum of GMR occurs for particle diameters around the electron mean free path. Varying the particle concentration, an optimum value is obtained around the percolation threshold.

Chapter 3

Preparation and characterization of the system

In this chapter the experimental apparatuses for both samples preparation and characterization are presented. A great deal of attention is given to the deposition technique used to make the films because it is a particular methodology that permits the thin film deposition out of the thermodynamic equilibrium. The films made in this thesis work are analyzed with different experimental techniques. Magnetic and magnetoresistive measurement are collected with a Superconducting Quantum Interference Device magnetometer(SQUID), operating in the 4-300 K temperature range at a maximum applied field of 50 kOe. This instrument allows the detection of very low signals, the resolution being of 10^{-6} emu, and for this reason it is suited to characterize samples containing low quantities of magnetic material. Structural investigation is made with the support of X-ray diffraction, in collaboration with prof. Michele Sacerdoti of the Department of Earth Science of Ferrara University and Mössbauer spectroscopy. In this chapter there are the description of the deposition technique and of the Mössbauer spectroscopy, for the other techniques used for the characterization of the samples there is

a brief description in the experimental chapter.

3.1 Experimental technique for the production of the samples

3.1.1 Dc-Magnetron Sputtering

Sputtering is a physical vapour deposition process used to deposit a film of atoms onto a substrate. Within the sputtering process gas ions out of a plasma are accelerated towards a target consisting of the materials to be deposited. A plasma is a primarily electrically neutral collection of free charged particles (electrons and one kind of positive ions) moving in the random directions. Material is detached from the target and afterwards deposited on the substrate in the vicinity. Target atoms are bombarded with a discharge by an energetic ion which dislodges them. In a high vacuum (10^{-7} torr), these atoms will disperse in random directions until they find a suitable substrate to land on and stick to. It is possible to grow a film of desired thickness by knowing the film growth rate and choosing the correct sputtering time. A plasma may be broadly defined as a quasineutral gas that exhibits a collective behaviour in the presence of applied electromagnetic fields. Plasmas are weakly ionized gases consisting of a collection of electrons, ions, and neutral atomic and molecular species. Artificial plasmas broadly differ in the density n (number per cm^3) of charged species, n is typically in between 10^7 cm^{-3} and 10^{20} cm^{-3}. The application of a sufficiently high DC voltage between metal electrodes immersed in a low-pressure inert gas initiates a discharge. In gases the process begins when a stray electron near the cathode carrying an initial current i_0 is accelerated toward the anode by the applied electric field (ε). After gaining sufficient energy the electron collides with a neutral gas atom (A) converting it into a positively charged ion (A+). During this

impact ionization process, charge conservation indicates that two electrons are released, i.e., $e^- + A \rightarrow 2e^- + A^+$. These are accelerated and now bombard two additional neutral gas atoms, generating more ions and electrons, and so on. Meanwhile, the electric field drives ions in the opposite direction so they collide with the cathode, ejecting, among other particles, secondary electrons. These now also undergo charge multiplication. The effect snowballs until a sufficiently large avalanche current ultimately causes the gas to breakdown. In order for breakdown to occur, the distance (d) between electrode must be large enough to allow electrons to incrementally gain the requisite energy for an ionization cascade. Also, the electrodes must be wide enough to prevent the loss of electrons or ions through sideways diffusion out of the interelectrode space. The Townsend equation

$$i = i_0 \frac{exp\ (\alpha d)}{[1 - \gamma_e\,(exp\ (\alpha d) - 1)]} \qquad (2.1)$$

reveals thet the discharge current (i) rises dramatically with respect to i_0 because of the combined effects of impact ionization and secondary electron generation. These processes are defined by constants α and γ_e, respectively. Known as the Townsend ionization coefficient, α represents the probability per unit length of a ionization process occurring during an electron-gas atom collision. γ_e is the Townsend secondary-electron emission coefficient and is defined as the number of secondary electrons emitted at the cathode per incident ion. For an electron of charge q traveling a distance α, the probability of reaching the ionization potential V_i is $exp - (V_i/q\varepsilon\lambda)$, so that

$$\alpha = \frac{1}{\lambda} exp \frac{-V_i}{q\varepsilon\lambda} \qquad (2.2)$$

We may associate λ with the intercollision distance or mean free path in a gas and it is in inversely proportional to the system pressure. The breakdown is assumed to occur when the denominator in Eq. 2.1 is equal to zero, i.e., when $\gamma_e(\exp(\alpha\ d)$ - 1) = 1, for then the current is infinite. From this condition plus

Eq. 2.2, the critical breakdown field ($\varepsilon = \varepsilon_B$) and voltage ($V_B = d\varepsilon_B$) can be calculated and expressed in terms of a product of pressure and interelectrode spacing. The result, known as Paschen's Law, is expressed by

$$V_B = \frac{APd}{ln(Pd) + B} \qquad (2.3)$$

where A and B are constants. The Paschen curve is a plot of V_B vs Pd (plotted in figure 3.1)

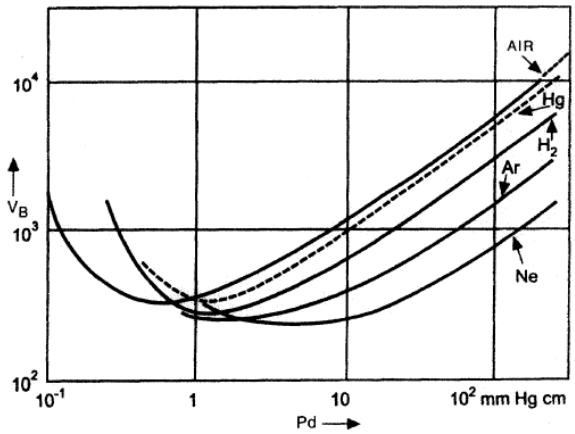

Figure 3.1: Paschen curves for a number of gases. From A. von Engel, Ionized Gases. Oxford University Press, Oxford, 1965

At low values of Pd there are few electron-ion collisions and the secondary electron yield is too low to substain ionization in the discharge. On the other hand, at high pressures there are frequent collisions, and since electrons do not acquire sufficient energy to ionize gas atoms, the discharge is quenched. Thus at both extremes, ion generation rates are low and high voltages are required to sustain the discharge. In between, at typically a few hundred to a thousand volts, the discharge is self-sustaining. This means that for each electron at the cathode, $exp(\alpha d)$ electrons reach the anode, and the net effect of the collisions is to produce a new electron at the cathode. Practically, however, in most sputtering discharges the Pd product is well to the left of the minimum value (see fig. 3.1).

The plasma is electrically neutral on average so that $n_e = n_i = n$ where n_e and $n_i = n$ are the density of electrons and ions, respectively. Collisions between neutral gas species essentially cause them to execute a random Brownian motion. However, the applied electric field disrupts this haphazard motion because of ionization. If the density of charged particles is high enough compared with the size of the plasma, significant coulombic interaction exists among particles. This interaction enables the charged species to flow in a fluid-like fashion that determines many of the plasma properties. The degree of gas ionization (f_i) is defined by $f_i = n_e/(n_e + n_0)$ where n_0 is the density of neutral gas species. f_i typically has a magnitude of $\approx 10^{-4}$ in the glow discharges used in thin film processing.

Motion of plasma: current and diffusion

Since surfaces (e.g., targets, substrates) are immersed in the plasma, they are bombarded by the species present here in. Charged particle impingement results in an effective electrical current density (j) given by the product of the particle flux ($\frac{1}{4}n\overline{v}$) and the charge (q) transported, where the factor of $\frac{1}{4}$ reflects that fraction of the random motion that is directed at the planar surface. Therefore,

$$j = \frac{n\overline{v}q}{4}$$

where n and $\overline{v}$ are the charged species concentration and mean velocity. Initially, an isolated surface within the plasma charges negatively because of the greater electron bombardment. Subsequently, additional electrons are repelled while positive ions are attracted. Therefore, the surface continues to charge negatively at a decreasing rate until the electron flux equals the ion flux and there is no net current. We now consider the mobility (μ) of charged species in the presence of an applied electric field (ε). The mobility is defined as the velocity per unit electric field or $\mu = v/\varepsilon$. Using Newton's

law,

$$m\ dv/dt = |q|\,\varepsilon + m\,[\delta v/\delta t]_c\,oll$$

where q is the species charge. The second term on the right reflects a kind of frictional drag that particles experience during motion because of their collisions with other particles. When the particle collides, it essentially loses memory of direction of motion. It is common to set $[\delta v/\delta t]_c\,oll = v\nu$, where ν is the collision frequency, a factor assumed to be constant for simplicity. In the steady state, $dv/dt = 0$ and $\mu = |q|/mv$. Typical mobilities for gaseous ions at 1 torr and 273 K range from $\approx 410^2 cm^2$/V-s (for Xe^+) to $1.1x10^4 cm^2$/V-s (for H^+). A second kinetic effect involving species motion in plasmas is diffusion, a phenomenon described by the Fick's Law. When migrating species move under the simultaneous influence of two driving forces, i.e., diffusion in a concentration gradient (dn/dx) and drift in the applied electric field, we may write for the respective electron and ion particle fluxes,

$$J_e = -n_e\mu_e\varepsilon - D_e\ dn_e/dx$$

$$J_i = -n_i\mu_i\varepsilon - D_i\ dn_i/dx$$

To maintain charge neutrality in the region under consideration it is assumed that $J_e = J_i = J$, and $n_e = n_i = n$. By the two previous expression s it is found that

$$\varepsilon = \frac{(D_i - D_e)}{n(\mu_e + \mu_i)}\frac{dn}{dx}$$

Therefore, it is apparent that an electric field develops because the difference in electron and ion diffusivities produces a nonzero charge density within the plasma. Physically, more electrons than ions tend to leave the plasma, establishing an electric field that hinders further electron loss but at the same time enhances ion motion. Because of the coupled electron and ion motions we can assign an effective ambipolar diffusion coefficient D_a to describe the effect,i.e.,

$$D_a = \frac{(D_i\mu_e + D_e\mu_i)}{(\mu_e + \mu_i)}$$

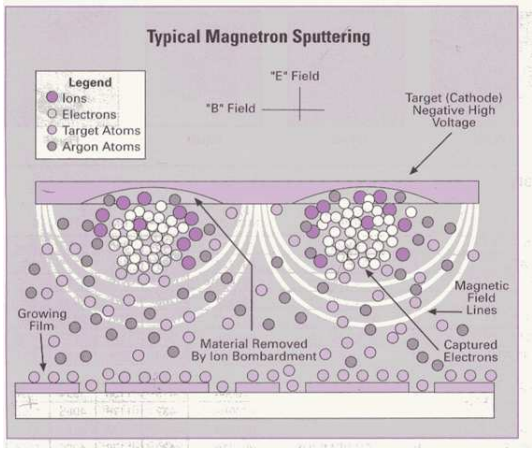

Figure 3.2: Deposition technique: *Dc* magnetron sputtering.

The magnitude of D_a lies somewhere between those of D_i and D_e so that both ions and electrons diffuse faster than intrinsic ions do.

The Sputter Parameters

The resulting film properties can be controlled by adjusting the following sputter parameters:

- the *sputter current* I_{sp} mainly determines the rate deposition and hence the average time that the impinging particles have for either surface diffusion and agglomeration on existing growth centers or nucleation with other adatoms;

- the *applied voltage* determines the maximum energy, which sputtered particles can escape from the target with (reduced by the binding energy). The energies of the sputtered particles show a broad distribution with a maximum of the distribution between 1 eV and 10 eV. The applied voltage determines also the sputter yield, which is the number of sputtered particles per incoming ion;

- The *pressure* p in the sputter chamber determines the mean free path

λ for the sputtered material, which is proportional to $1/p$;

- Together with the $target - substrate\ distance$ (d) the pressure determines how many collisions occur for the particles on their way from the target to the substrate. This can affect the porosity of the films, their crystallinity and their texture, as well [26];

- The $Ar - flow$ is the parameter varied whereas the total pressure is kept constant;

- The *substrate temperature* can have a strong impact on the growth for what concerns the crystallinity or the density of the samples. It can be adjusted between room temperature and 500°C. But even without external heating, the substrate temperature may rise considerably, especially when long sputtering times;

In principle a bias-voltage can be applied to the substrate up to ±100V, and has the effect of accelerating electrons or ions towards the substrate or keeping them away from it. Both may have an influence on the layer growth [27, 28]. Usually substrate and target surface are parallel to each other. A variation of the deposition angle can be achieved by tilting the substrate. Thereby a new preferential direction for the film growth and potentially anisotropic films can be produced.

Magnetron Sputtering

Magnetron sputtering is the most widely used variant of DC sputtering. To increase the ionization rate by emitted secondary electrons even further, a magneto below the target is used. The electrons in its field are trapped in cycloids and circulate over the target surface, so they not damage the samples and it is reduced the disordered effect of the electrons on the growth of the film.

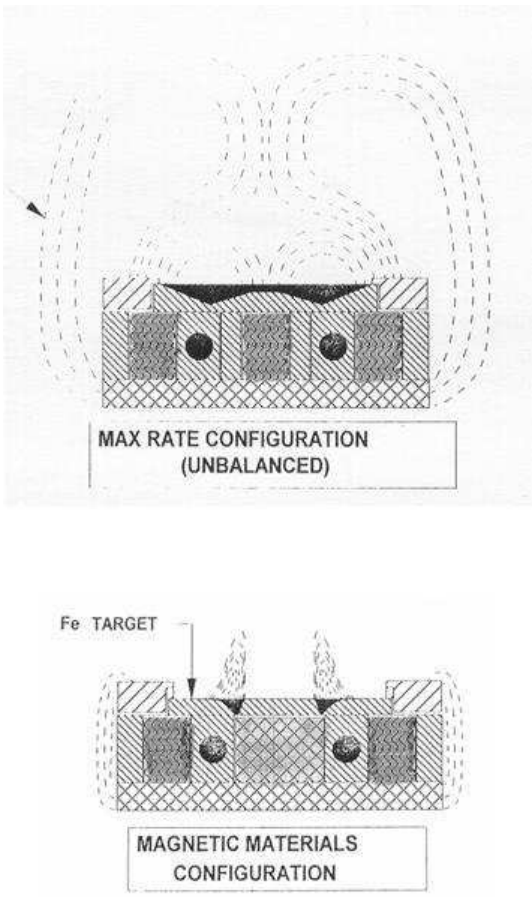

Figure 3.3: Magnetic field around the Ag (up) and Fe (down) target.

One to two orders of magnitude more current is typically drawn in magnetron than simple DC discharges for the same applied voltage. Important implications of this are higher deposition rates or alternatively, lower voltage operation than for simple DC sputtering. Another important advantage is reduced operating pressures. At typical magnetron-sputtering pressures of a few millitorr, sputtered atoms fly off in ballistic fashion to impinge on substrates. Avoided are the gas phase collisions and scattering at high pressures which randomize the directional character of the sputtered-atom flux and lower the deposition rate. A fundamental reason for these beneficial effects

in magnetrons is the displacement of the Paschen curve to lower Pd values relative to simple discharges. Therefore, for the same electrode spacing and minimum target voltage a stable discharge can be maintained at lower pressures. The configuration of the magnets, placed under the target, is presented in figure 3.3. The first configuration (low bias) is for non magnetic material. It reduces the energy of the electrons moving toward the substrate below the energy of the first ionization potential for Ar. Deposition rates are low but more careful. The second configuration is for the magnetic materials. It optimizes saturation of the magnetic target material thereby allowing some field lines to extend above the target surface.

3.1.2 Quarz Oscillator

For the deposition rate evalutation it is used a microbalance that measures the deposited quantity on the surface of a crystal quartz. If the material density is known, it is possible to convert the mass into the thickness of the deposited film. The QCM (*Quartz Crystal deposition Monitor*) relies on the piezoelectric sensibility of the quarz crystal. When on the crystal surface is deposited a mass, the resonance frequency is reduced and the frequency variation ΔF is correlated to the mass of material depositated on the surface:

$$\frac{M_f}{M_q} = \frac{\Delta F}{F_q}$$

where M_f is the mass deposited on the quarz, M_q and F_q are the mass and the frequency of the quarz before the deposition. Note the material density d_f, the density of the quarz d_q and the cut frequency AT N_{at}, with simple substitutions it is possible to find the thickness of the deposited materials T_f:

$$T_f = 4.4 \cdot 10^5 \frac{\Delta F}{F_q^2 \cdot d_f}$$

In this way it is possible to determine the thickness of the deposited materials on a quarz crystal using the measurement of the crystal frequency variation.

The resonance frequency is AT because the temperature variation not much influence. With the quarz microbalance, besides the thickness of the samples, it is used to fix the relative concentration of the two metals during the co-deposition, after the exact concentration is examined with Rutherford Backscattering Spectroscopy.

3.2 Experimental technique for the characterization of the samples

The experimental technique used for the characterization of the samples are numerous: resistive measurements are collected with the four probe method in Van Der Pauw configuration, the magnetic measurement with SQUID magnetometer and structural investigation are carried out with X-ray diffraction and Mössbauer spectroscopy. In this chapter the Mössbauer spectroscopy is described.

3.2.1 Mössbauer spectroscopy

Mössbauer effect is the recoil-free emission of a γ photon by a radioactive nucleus and the subsequent resonant recoil-free reabsorption by another nucleus. In the process, the source nucleus goes from the excited state down to the ground state and the absorber nucleus in the ground state is raised into the excited state. In the transition from the excited state to the ground state no energy is lost to the system, and the γ-rays carries the total energy of this transition. The excited state has a mean lifetime τ or half lifetime $t_{1/2} = \tau ln2$. If the ground state is stable, or has a long lifetime and its energy level is well defined. The natural line width ofthe source emission or the absorption line is $\Gamma = \hbar/\tau = 0.693\hbar/t_{1/2}$. The line width is defined as the full width at half maximum. The first excited state of Fe^{57} (14.4 KeV) has a value

of $t_{1/2} \approx 10^{-7}$ sec, thus the natural line width is $\Gamma \approx 5 \cdot 10^{-9}$ eV. The magnitude of characteristic phonon energies, $h\nu_D = k_B\theta_D$ of typical solids and the recoil energies E_R in low energy γ-emission or absorption are the same order of magnitude while for the significance and relative accurancy of the effect the large distance between γ-ray energy E_γ and line width Γ is decisive. The lifetime of the excited state or the natural line width is the characteristic time in Mössbauer spectroscopy. The sharpness and the position of the Mössbauer is most important to determine the energy positions of the emitted γ-ray from a source relative to an absorber with a high degree of accurancy. There are two main contributions of great significance: the hyperfine interaction and relativistic effects. The hyperfine interaction consists of interactions between a nuclear property and an appropriate electronic or atomic property. There a re three main hyperfine interactions corresponding to the nuclear moments determing the nuclear levels: a) Electric monople interaction (isomer shift); b) electric quadrupole interaction (quadrupole splitting); c) magnetic dipole interaction (nuclear Zeeman effect). The isomer shift (δ) arises due to the non-zero volume of the nucleus and the electron charge density due to s-electrons within it. This leads to a monopole (Coulomb) interaction, altering the nuclear energy levels. Any difference in the s-electron environment between the source and absorber thus produces a shift in the resonance energy of the transition. This shifts the whole spectrum positively or negatively depending upon the s-electron density, and sets the centroid of the spectrum. As the shift cannot be measured directly it is quoted relative to a known absorber. For example ^{57}Fe Mössbauer spectra will often be quoted relative to α-iron at room temperature. The isomer shift is useful for determining valency states, ligand bonding states, electron shielding and the electron-drawing power of electronegative groups. For example, the electron configurations for Fe^{2+} and Fe^{3+} are $(3d)^6$ and $(3d)^5$ respectively. The ferrous ions have less s-electrons at the nucleus due to the greater screening of the

d-electrons. Thus ferrous ions have larger positive isomer shifts than ferric ions.

Nuclei in states with an angular momentum quantum number $I > 1/2$ have a non-spherical charge distribution. This produces a nuclear quadrupole moment. In the presence of an asymmetrical electric field (produced by an asymmetric electronic charge distribution or ligand arrangement) this splits the nuclear energy levels. The charge distribution is characterised by a single quantity called the Electric Field Gradient (EFG). In the case of an isotope with a $I = 3/2$ excited state, such as ^{57}Fe, the excited state is split into two substates $m_I = \pm 1/2$ and $m_I = \pm 3/2$ (figure 2.1). The magnitude of splitting, Δ, is related to the nuclear quadrupole moment, Q, and the principle component of the EFG, V_{zz}, by the relation $\Delta = eQV_{zz}/2$.

The interaction of the nuclear magnetic dipole moment μ with a magnetic field H at the site of the nucleus, splits the nuclear state with spin I ($I > 0$) into ($2I$+1) sublevels with the eigenvalues (Zeeman splitting):

$$E_m = -\frac{\mu H m_I}{I} = -g_N \beta_N H m_I$$

where m_I is the magnetic quantum number with the values $m_I = I, I - 1, ..., -I$. The nuclear magnetic moment is related to the nuclaer Bohr magneton $\beta_N$by the nuclear Land splitting factor g_N

$$\mu = g_N \beta_N I.$$

There are many sources of magnetic fields that can be experienced by the nucleus. The total effective magnetic field at the nucleus, B_{eff} is given by: $B_{eff} = (B_{contact} + B_{orbital} + B_{dipolar}) + B_{applied}$ where the first three terms being due to the atom's own partially filled electron shells. $B_{contact}$ is due to the spin on those electrons polarising the spin density at the nucleus, $B_{orbital}$ is due to the orbital moment on those electrons, and $B_{dipolar}$ is the dipolar field due to the spin of those electrons. Transitions between the excited state

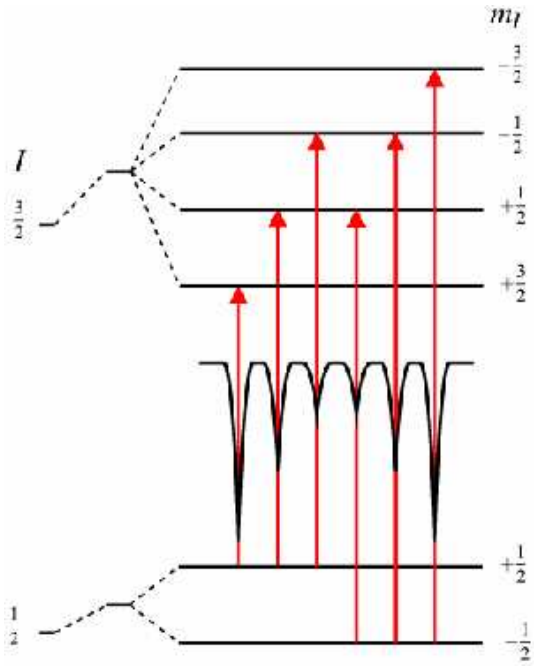

Figure 3.4: Magnetic splitting of the nuclear energy levels.

and ground state can only occur where m_I changes by 0 or 1. This gives six possible transitions for a 3/2 to 1/2 transition, giving a sextet in figure 3.4, with the line spacing being proportional to B_{eff}. The line positions are related to the splitting of the energy levels, but the line intensities are related to the angle between the Mössbauer γ-ray and the nuclear spin moment. In single crystals or under applied fields the relative line intensities can give information about moment orientation and magnetic ordering.

So Mössbauer spectra are described using three parameters: isomer shift, δ, which arises from the difference in s electron density between the source and the absorber, quadrupole splitting, Δ, which is a shift in nuclear energy levels that is induced by an electric field gradient caused by nearby electrons, and hyperfine splitting (for magnetic materials only). Graphically, quadrupole splitting is the separation between the two component peaks of a doublet (see figure 3.5), and isomer shift is the difference between the mid-

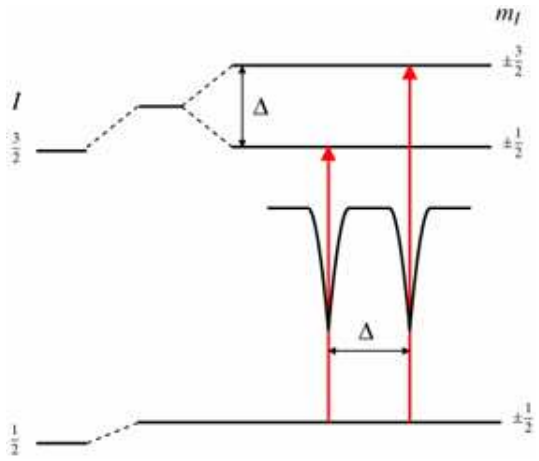

Figure 3.5: Quadrupole splitting for a 3/2 to 1/2 transition. The magnitude of quadrupole splitting, Δ, is shown.

point of the doublet and zero on the velocity scale. Mössbauer parameters are temperature-sensitive, and this characteristic is sometimes exploited by using lower temperatures to improve peak resolution and induce interesting magnetic phenomena. If the electrons around the Fe atom create a magnetic field, as in the case of magnetite, then the energy levels in the Fe nucleus will split to allow six possible nuclear transitions, and a sextet (six-peak) spectrum results. The positions of the peaks in the sextet defines what is called the hyperfine splitting of the nuclear energy levels (figure 3.4)

In the hyperfine interaction pattern, time dependent features are often observed. The fluctuating fields causing broadening can be described by a correlation time characterizing various relaxation processes. In the case of superparamagnetism the net magnetization of single domain particles fluctuates thermally between different easy directions for sufficiently small particles. In the presence of a paramagnetic hyperfine interaction, the following two characteristic times have to be considered: the relaxation time of the electron spin (spin-spin and spin-lattice) τ_S and the nuclear Larmor precession time τ_L. If $\tau_S \gg \tau_L$, astatic nonvanishing hyperfine interactionis present at the

nucleus and a hyperfine spectrum with sharp lines is expected. If $\tau_S \ll \tau_L$, the hyperfine interaction produces an average value as a result of he rapidly fluctuating electron spins and the splitting collapses. Under the condition $\tau_S \approx \tau_L$ complicated spectra with broad lines are found which allow an estimate of the electron relaxation time to be made. This technique have some advantage. The measurement is a local measurement. The spectrum result from a measurement arises from a superposition of local effects, not from the average. Moreover the measurement can be achieved without applying a field and it is performed along any direction, not along one particular direction as in the case of magnetic measurement. Moreover, the timescale is thus rather short and yet long enough to allow observation of the blockade state to superaramagnetic state transition in a convenient temperature range. Mössbauer atoms with different surroundings give distinct signal.

Chapter 4

Experimental results and discussion

This chapter is devoted to experimental results, their analysis and discussion. At first, the investigated system and the deposition parameters are presented. Afterwards, the magnetoresistive and magnetic measurement performed at room temperature and discussed in order to elucidate how the system changes with the ferromagnetic metal concentration. To understand how these properties (magnetic and magnetoresistive) were correlated with the structure of the samples, structural investigation with X-ray diffraction and Mössbauer spectroscopy was performed. The results of these measurement helped to explain the best arrangement of the structure to obtain the greatest of the GMR efficiency of the system. Subsequently a low temperature and low field analysis was executed investigate the origin of magnetic interactions in the system whose presence was pointed out by the correlation between magnetic and magnetoresistive measurements. In conclusion all the presented results are discussed and a picture of the nanoscale morphology of the system that features the highest GMR efficiency is suggested.

4.1 The Fe-Ag system

The samples are prepared by *dc* magnetron sputtering in co-sputtering configuration because the material (Fe and Ag) have a negligible solubility [29], in this way the two materials do not form an alloy, a low efficacy system for GMR observation, but a magnetic nanoparticles dispersed in the matrix of the non magnetic material, so it is necessary to use a deposition technique out of the thermodynamical equilibrium. *Dc* magnetron sputtering is one of the method that permits the growth of a sample with fine Fe particles embedded in Ag matrix, because with different methods, like, for example, rapid solidification, the two material properly do not intermix and give rise to large precipitates [30].

Fe_xAg_{1-x} samples were deposited on a Si substrate in Ar atmosphere. x represents the Fe atomic concentration. It was adjusted by changing the Fe and Ag growth rates and ranges from 0.1 to 0.5 because in this range the maximum of GMR may be expected while in both Fe-poor and Fe-rich regions GMR is substantially suppressed [31]. The Fe and Ag growth rates and the thickness of the deposited films was determined by a quartz microbalance and it is about 250 nm. The substrate was rotated during the deposition to obtain a uniform thickness. The background pressure before deposition was 10^{-7} torr and the Ar sputtering pressure was kept at 10 mTorr by a feedback gas-flow controller. The FeAg samples were analysed with the Rutherford Backscattering Spectrometry (RBS) to estimate the exact atomic concentration of Fe in Ag and the sample thickness. The surface of the samples result partially oxidized, impurities like oxygen, hydrogen or nitrogen was detected at the surface, this is possible even if the samples were conserved in controlled atmosphere (argon). Another possibly impurity is argon that it is a consequence of the method deposition. In fact scanning the samples with AFM (atomic Force Microscopy) they reveal a raised roughness, so the

surface oxidized results higher. The layer below instead were resulted devoid of impurities.

4.2 Study at room temperature of the samples as a function of the concentration

The magnetoresistive effect as a function of the external magnetic field is presented in figure 4.1 for different values of the Fe atomic concentration (x) at room temperature. The maximum applied magnetic field is 1.3 T. The MR curve, for low Fe concentration, has a parabolic shape, typical of a system of superparamagnetic particles; instead, for high concentration ($x > 0.30$) the curve has a rapid response at low field and for high magnetic fields an approach to saturation can be observed.

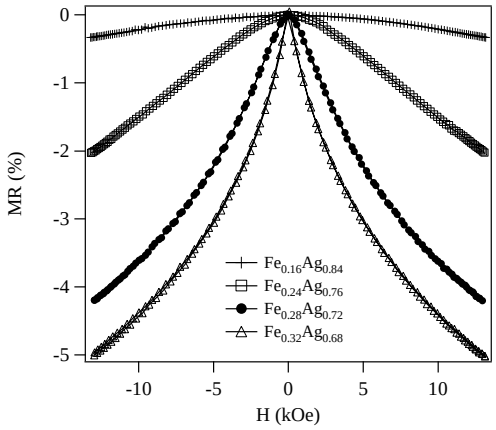

Figure 4.1: GMR dependence on magnetic field measured at room temperature for samples as a function of x.

In figure 4.2 the dependence of GMR as a function of H for some samples in the different measurement configuration of Van Der Pauw method is presented. The different configuration are three: H parallel to the plane of the sample, one with H parallel and the other with H perpendicular to the

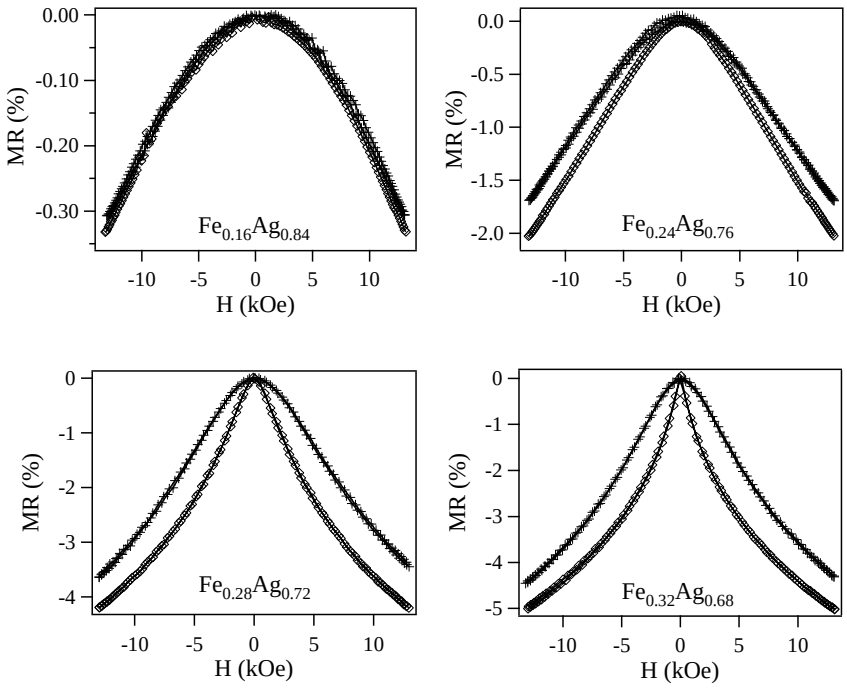

Figure 4.2: MR dependence on H for various concentration of Fe in two different measurement configuration: ◊ for H parallel and + for H perpendicular to the film.

current; the third is with H perpendicular to the plane of the sample. In figure 4.2 is presented only two configuration (one with H parallel to the film and one with H perpendicular to the film) because the two configurations with H parallel to the film are equal. Looking the graph in figure 4.2 it is clear that for the sample with low x the three configuration are equal, to confirm the superparamagnetic behaviour. Increasing the Fe concentration, the measurements with H perpendicular differ from the other, so a plane anisotropy is present and it increase with x. So it is possible that increasing x the Fe clusters have a non spherical shape, even it is associate with the deposition technique [32].

In figure 4.3 there is the trend of GMR as a function of x. The GMR effect increases with x up to $x = 0.32$. In the granular system, GMR effect

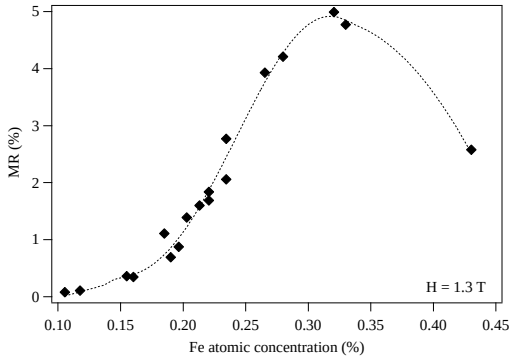

Figure 4.3: GMR dependence on Fe concentration measured at 1,3 T: ♦ are the experimental data for the samples as deposited. Line is a guide to the eye.

depends on the number of Fe atoms in the samples [33]. The Fe concentration changes both the scattering centres density (enhances GMR) and the magnetic interactions (decreses GMR). To understand which is the interplay of these two effects due to the specific magnetic morphology of the samples a magnetic and structural investigation is needed.

The magnetic measurements were collected at room temperature with a Squid magnetometer whit a maximum magnetic field of 5 T. The MvsH plots for different Fe concentration are presented in figure 4.4. The response changes with the Fe concentration, in fact also for low x the curve is a typical Langevin with a slow response for low fields. For high fields the magnetization does not saturate. With increasing the Fe concentration, the magnetic response changes, in fact at low fields the slope of the $MvsH$ curve increases. For all the concentration, in the MvsH curve the coecitive field is zero. Using a linear combination of Langevin functions it is possible to make a fit of the magnetization curve and evaluate the magnetic volume of the clusters in the samples. For samples with low Fe concentration just one Langevin curve is enough for a good fit, this can be interpreted as the presence of just one average magnetic volume; for high Fe concentration ($x > 0.2$) it is

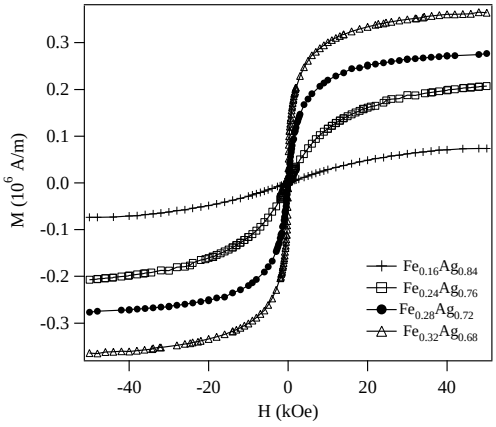

Figure 4.4: Magnetization dependence on magnetic field at 300 K for different Fe concentrations.

necessary to use at least two Langevin contributions. The cluster magnetic size is about a few nanometres for low x, but increasing the Fe amount the size considerably increases, up to a few tens of nanometres. Comparing these values with the clusters size deduced from the fit of MRvsH curves with the square of Langevin curve, it is clear that the magnetic size is not the real Fe cluster size but it is the counterpart of the magnetic interactions increasing, because the values obtained from MR data are lower, so volumes deduced by the magnetic measurements are the magnetic region size.

A superparamagnetic system shows a linear dependence between the magnetoresistance and the squared reduced sample magnetization [12]:

$$GMR(M/M_{sat}) = \gamma(M/M_{sat})^2$$

In figure 4.5 the $MRvs(M/M_{sat})^2$ dependence for different Fe concentrations is presented. The expected trend is a straight line. For low concentration the trend is a line but for high magnetic field it deviates from linearity. For high concentration instead the trend diverges from line for every value of magnetic field. These differences from the linear expected behaviour are explainable with the presence of both a volume distribution and magnetic interactions

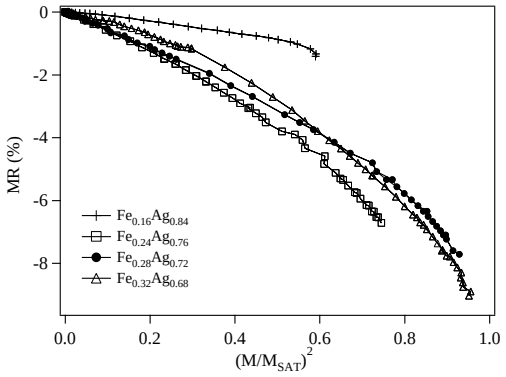

Figure 4.5: The trend of $MRvs(M/M_{sat})^2$ for samples with different Fe concentration.

between the Fe cluster. In fact the volume distribution increase the MR effect, because the presence of clusters (polydisperse sample) with size smaller that the mean size leads to increase MR value relative to monodisperse sample [19, 25]. The dipolar interaction, instead, may cause a strong reduction of the GMR effect in particular the reduction is larger for a polydisperse volume distribution. In fact, the deviations from the straight line is produced by the differentiation in the response of the various clusters to the applied field. When the dipolar interactions are present, deviations from linear dependence occur which are more severe for the polydisperse system [25].

γ can be interpreted as the overall GMR variation in correspondence with a unit change of reduced squared magnetization, so can be seen as a global indication of how effective is the granular structure in producing GMR. The maximum of γ is observed for $x \sim 0.26$, so this is the concentration where there is the maximum of the efficiency of the system also if there is not the concentration with the maximum MR effect. γ can be also thought as a function of M/M_{sat}:

$$\gamma(M/M_{sat}) = \frac{\partial GMR}{\partial (M/M_{sat})^2}$$

With this definition, γ in principle can change with M/M_{sat}; as a consequence

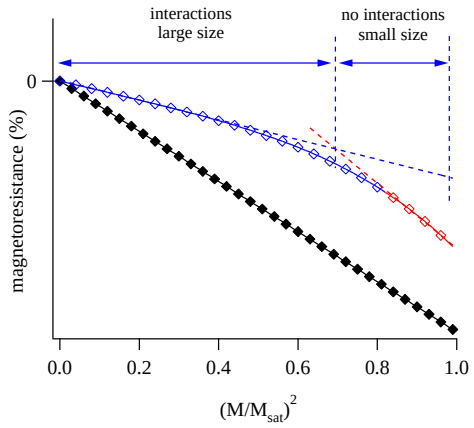

Figure 4.6: $MRvs(M/M_{sat})^2$ trend for a superparamagnetic system (⧫) and for an interacting system (◊).

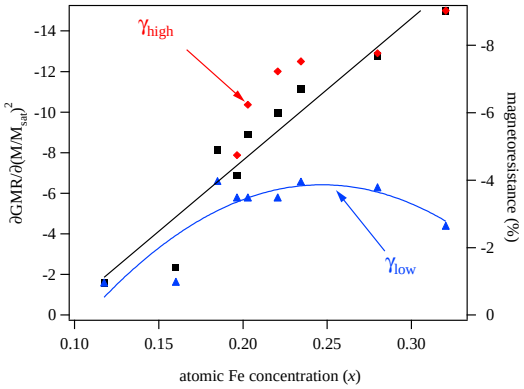

Figure 4.7: The trend of the parameter γ_{low} (▲) and γ_{high} (⧫) as a function of x, in comparison with MR (■).

of that, γ gives a local (i.e. specific of a given M/M_{sat} value) indication of the GMR efficiency of the considered sample.

For $M/M_{sat} \simeq 0$ the contribution of largest particles is dominant but for $M/M_{sat} \approx 1$ the aggregates with small size are dominant. In fact the Langevin function depends on $(\mu H/kT)$, where $\mu = VM_{sat}$, so it is clear that $V \propto 1/H$. γ_{low} is calculated within the low magnetization region, thus

it reveals GMR contributions originating from changes in the magnetic configuration that are generally characterized by large length scales (e.g. large particles or long range interactions), Differently, γ_{high} is obtained from the $M/M_{sat} \approx 1$ region, so it is due to GMR contributions originating from changes in the magnetic configuration that are characterized by small length scales (e.g. small particles or short scale Fe density fluctuations) (see figure 4.6). If we consider γ_{low}, namely γ measured for low $(M/M_{sat})^2$ values, we can study its dependence on x and compare it with the dependence of GMR on the same parameter. If, for a given x, γ does not change with $M/Msat$, as GMR turns out to be proportional to M^2, we expect to observe that GMR$\sim (M/M_{sat})^2$. On the other hand, if γ is affected by M, GMR and γ_{low} are decoupled and therefore their dependence on x may be different. In this case, we expect the γ_{low} dependence on x to deviate from the γ_{high} one. As can be seen in figure 4.7, for low iron concentration γ_{low} follows the GMR dependence on x. This indicates that in this regime both terms increase proportionally to Fe volume fraction. Therefore, from the point of view of these high field data, we are in a diluted regime, where the GMR spin-dependent scattering sources just increase in density without substantially changing their mutual interaction. For $x > 0.20$, GMR and γ_{low} separate, thus indicating that the density of spin dependent sources is still increasing (GMR grows with x) but that their mutual interaction is stronger, namely their effective magnetic volume gets larger. Fe nanoparticles do not touch with each other but they progressively lose their magnetic individuality owing to the magnetic interactions. So the FeAg system can be modelled as an ensemble of large magnetic grains made of smaller interacting Fe particles [34].

4.3 Study of the samples at low temperature

Analogous measurement at low temperature (4K) were made. The dependence of GMR as a function of H is presented in figure 4.8. The response of the samples at low temperature is different with respect to that observed at 300 K, as can be seen in figure 4.9 for the sample $Fe_{0.24}Ag_{0.76}$, moreover, the intensity of the GMR effect measured at 5 T is higher at low temperature. At low field the response is more quick and for high field there is

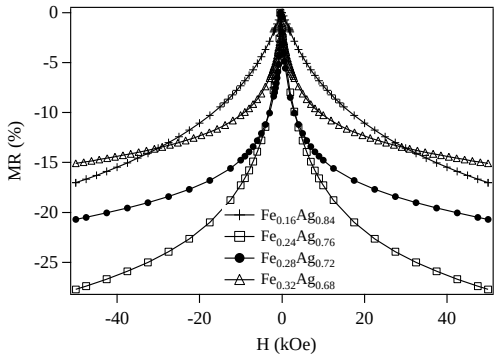

Figure 4.8: GMR dependence on magnetic field measured at 4 K for samples as a function of x.

an approach to saturation that at room temperature is not observed. Besides, as can be seen in figure 4.10, the maximum magnetoresistive effect at low temperature is found at a Fe concentration that is lower with respect to that where the maximum of GMR was observed at 300 K ($x \approx 0.22$). This confirms the presence of magnetic interactions that at low temperature are more strong. In fact the maximum shift indicates a drop of electrons spin scattering centres that decreasing the GMR.

Also the susceptibility response at 4 K is different from the trend observed at room temperature, as in this case there is a quick response at low value of magnetic field. The magnetic loops, made at 4 K, are presented in figure 4.11. The low field response is very quick, in fact the samples trend to

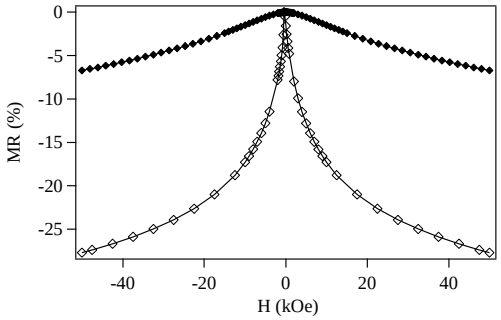

Figure 4.9: The trend of magnetoresistance in function of magnetic field for the sample $Fe_{0.24}Ag_{0.76}$ measured at 300 K (♦) and 4 K (◊).

saturation for low field values. The saturation magnetization is higher with respect to the value measured at 300 K. At 4 K, the GMR dependence on x more closely resembles the $\frac{\partial GMR}{\partial(m/m_{sat})^2}$ one (figure 4.10). The room-temperature monotonous GMR behaviour is not observed, as a maximum is found for $x \approx 0.20$. This feature can be ascribed to the presence of the magnetic percolation threshold (see figure 4.10), above the percolation limit Fe particles lose their magnetic individuality [34], as the magnetic size of the aggregates was found to increase with decreasing temperature.

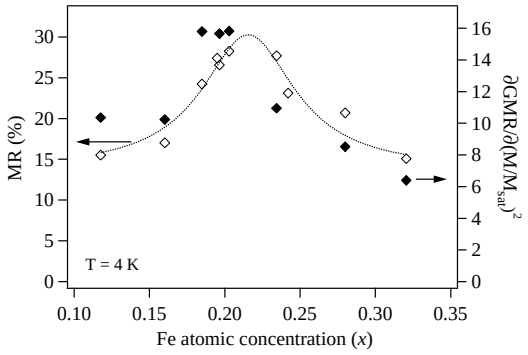

Figure 4.10: The trend of MR (left axis) and of $\frac{\partial GMR}{\partial(m/m_{sat})^2}$ (right axis) as a function of x.

After crossing this threshold, $\frac{\partial GMR}{\partial(m/m_{sat})^2}$ rapidly decreases, confirming that

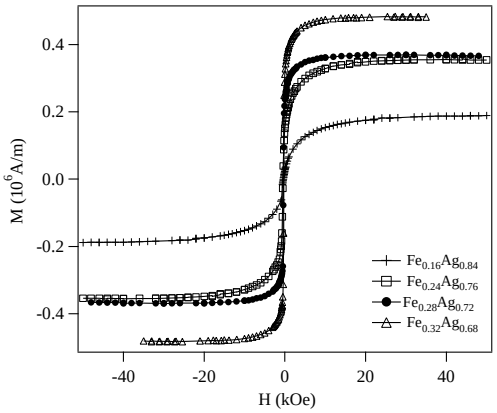

Figure 4.11: Magnetizazion dependence on magnetic field at 4 K for different Fe concentration.

the growth of system magnetic length scale is a decisive contribution to GMR intensity. On the other hand, if we consider the effect of the concentration on the γ_{high} value, we observe that it displays a remarkable increase for large values of x. This indicates that the system is not homogeneous and that the typical magnetic length scales are reduced by the increase in H [34]. In particular, short range scale magnetic changes in the magnetic configuration of the systems turn out to be effective in producing a change in samples resistance, even if they are due to regions that from the magnetic point of view represent just a small fraction of the samples. This may be due both to their small size and to the fact that they are embedded in a magnetic environment that is close to saturation, so the electronic current may be highly polarized [23].

4.4 Structural investigation

As a first step the structural texture of the Ag film produced by *dc* magnetron co-sputtering method was investigated. The XRD data were collected in the range between 35 and 50 degrees of 2θ because for higher angles the

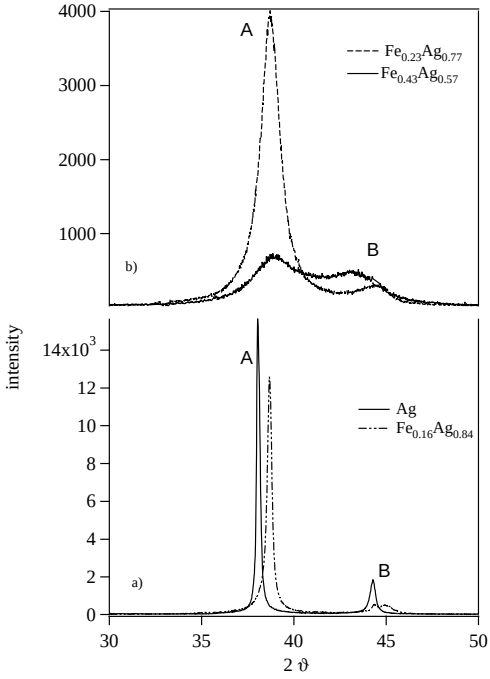

Figure 4.12: The XRD data for some sample. In the picture a) there are the XRD data for Fe_0Ag_1 and $Fe_{0.16}Ag_{0.84}$; in the picture b) there are the XRD data for $Fe_{0.23}Ag_{0.77}$ and $Fe_{0.43}Ag_{0.57}$.

Si reflections cover up the samples signal. As can be seen in figure 4.12a (full line), two main peaks A and B are found that we can interpret as the (111) and the (200) reflections of the Ag lattice. The lattice parameter is the same of the Ag bulk but the intensity ratio of these two peaks is not that expected for a polycrystalline Ag sample. We concluded that Ag crystals mainly grows with the [111] direction perpendicular to the growth plane [35]. After that, we collected the XRD spectra of the Fe_xAg_{1-x} films in the same angular range to examine how the angular position of the A and B peaks changes with x (figure 4.13). As can be seen in figure 4.13, we observe that as x increases the peak A shifts toward higher angle and go to the saturation, while the peak B first increases up to $x = 0.2$, than starts to decrease sharply finally to stabilize for $x = 0.32$. So we can distinguish three regimes.

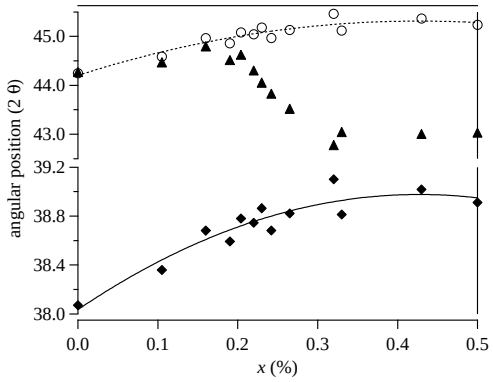

Figure 4.13: Angular position dependence of the first two peaks of XRD spectra as a function of atomic Fe concentration: ■ is the position of the peak (111), ▲ is the position of the peak (200). Line is the fit of the experimental data.

In the first regime ($x < 0.2$) the angular position of the peaks A and B increases with x so the lattice parameter of the samples decrease. Moreover, A and B width increases with x. The XRD data suggest therefore that the fcc structure of matrix changes when x increases because the presence of Fe atoms limits the growth of matrix grains, as can be seen in figure 4.13. In fact also the size of grains into samples, deduced with the Scherrer formula [36] from the full width at half maximum (FWHM) of the peaks, considerably decreases because the Fe presence keep Ag crystals from increasing their size. This view is supportated by the findings reported in a previous work [37]. The trend of the average grains size as a function of x resembles that of the lattice parameter. So we can interpret these results as if the structure of the samples in this region were similar to a Fe-Ag not-saturated solid solution, because the peak position continues to shift to higher angles with increasing x, with Fe atoms that occupy sostitutional position in the Ag lattice (fcc) and small Fe precipitates. The Vegard's law [38] say that a linear relation exists, at constant temperature, between the crystal lattice parameter of an alloy

and the concentrations of the constituent elements, like happen in the first region (figure 4.13). The presence of Fe cluster is confirmed by the presence of magnetic signal also for samples with low Fe content [39]. This is in contrast with another work [40], where, in the case of dc-sputtering, selected-area electron diffraction measurement showed that a metastable solid solution is observed for low Fe concentration and the formation of Fe cluster takes place only when the concentration increases. This confirms that Fe precipitates are small and diffraction spectra don't show a Fe contribution for low x. In the second regime ($0.2 < x < 0.32$), A continues to shift toward higher angles as x increases, and the lattice parameter comes to a minimum value. Moreover, B moves in the opposite direction with respect A to confirm that there is another contribution different to Ag lattice. It is reasonable to think that this can be due to the presence of Fe contribution. Therefore, the increase of Fe concentration supports the formation of iron clusters in a not-saturated Fe-Ag solid solution. Afterwards, for $x > 0.2$ A represents the contribution of the Fe-Ag solid solution and B is a mix of the contribution of Fe-Ag solid solution and the Fe clusters. In the third stage ($x > 0.32$), the intensity of B peak becomes comparable with the A one and the angular position of the peaks A and B remain constant. The lattice parameter trend is in agreement with a previous study [41]. We think that in this stage there is a saturated solid solution Fe-Ag and a new phase appears that we believe to be the contribution of Fe bcc. To check this hypothesis, we made a sample with large Fe concentration ($Fe_{0.50}Ag_{0.50}$) on a different substrate: Si (100) off 8^o in order to remove the diffraction peak (400) of Si from the spectra so we can analyze the position of other possible diffraction peaks as far as 80 degrees where in the spectra of the samples grown on Si(100) there is the Si reflection. In figure 4.14, the diffraction spectrum of the samples $Fe_{0.50}Ag_{0.50}$ is shown.

As see, B intensity is exceptionally high compared to A, which is approx-

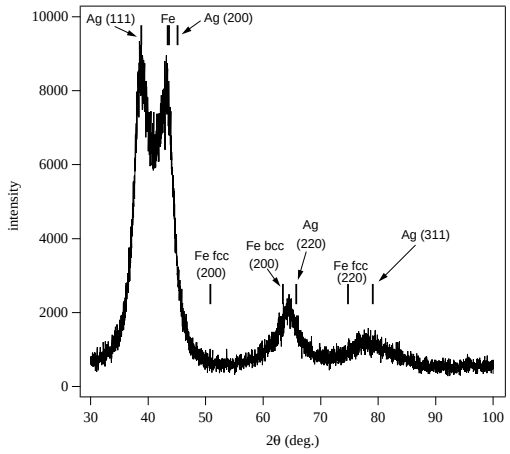

Figure 4.14: The XRD data for the sample $Fe_{0.50}Ag_{0.50}$. The | are the theorical position of the peak of Fe and Ag.

imately equal to A one, which could indicate that it includes also a Fe peak. In fact, considering that Fe grows spontaneously bcc, for low concentration of Fe it is reasonable to suppose that Fe grows fcc on the matrix structure, so it is not detectable with diffraction measurement. Instead, increasing x, it is possible that Fe grows bcc. Considering B position as the first reflection of Fe bcc, with dilated lattice parameter for the presence of Ag atoms in the lattice, we can calculate where the angular position of the other reflections are expected: as you see in figure 4.14 we have detected the (200) Fe-bcc. So the new phase could be a reflection of the Fe-bcc cluster. This is in agreement with previous work [35], they grow a Fe-Ag alloy with tandem deposition, and they showed that in this particular samples there is only the bcc phase in the Fe-rich region ($x > 0.86$) and only the fcc phase in the Ag-rich region ($x < 0.4$); in the middle there are a fcc phase and an amorphous phase.

Apart from the influence of temperature dependent interactions effect, shown in § 3.2, the major changes in GMR intensity and γ take place when the system structure turns from an Fe-Ag solid solution to a Fe-Ag solid solution with Fe precipitates. This indicates that the dispersion of small Fe pre-

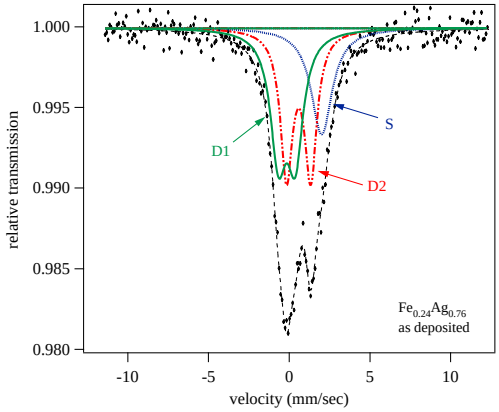

Figure 4.15: Mössbauer data (solid symbols) and fit (dotted line) for the $Fe_{0.24}Ag_{0.76}$ as deposited. Straight lines represent the three contributions used to fit the data to the model presented in the text.

Contribution	IS (mm/s)	QS (mm/s)	Fe rate
singlet (S)	0.50 ± 0.05	/	23%
doublet one (D1)	-0.04 ± 0.01	8.07 ± 0.29	39%
doublet two (D2)	0.15 ± 0.007	5.64 ± 0.52	38%

Table 4.1: Isomeric shift (IS) and the quadrupole splitting (QS) of fit of Mössbauer spectra for the sample $Fe_{0.24}Ag_{0.76}$ before the thermal treatment

cipitates and/or single atoms within the Ag matrix is the system that shows the highest GMR change per unit magnetization. Indeed, this kind of sample possibly displays the highest density of weakly correlated spin-dependent scattering sources. Moreover, the cluster glass interactions may favour a zero-field disordered magnetic configuration, a condition that enhances GMR. To investigate the arrangement of the Fe atoms we used Mössbauer spectroscopy. We analysed one sample with $x < 0.2$ ($Fe_{0.16}Ag_{0.84}$), one with $0.2 < x < 0.32$ ($Fe_{0.24}Ag_{0.76}$) and the sample with $x = 0.32$ that has the maximum of GMR. The spectrum of the sample $Fe_{0.24}Ag_{0.76}$ has been reported in figure 4.15. Ev-

ery sample shows a slightly asymmetrical doublet structure and the asymmetry changes and increases with x. The presence of a sextet contribution is not observed, so the Fe agglomerates don't have a stable magnetic moment with respect the very short Mössbauer measurement time ($10^{-8} sec$) so the magnetic structure shows a mainly superparamagnetic character [42, 43]. The experimental spectrum was fitted taking into account the results obtained with X-ray diffraction measurements. Three contributions were considered [44], each representing a different Fe chemical environment: singlet (S) arising from Fe atoms in Fe-Ag solid-state solution and two doublets arising from bcc-Fe cluster ascribed to atoms of core (D1) and to atoms at surface (D2). The isomer shift (IS) of D1 is always zero and the number of aggregate increases with x because the contribution of D1 increase, in agreement with our diffraction measurements and with previous study [45]. In particular we analyse the spectra of the sample $Fe_{0.24}Ag_{0.76}$ (figure 4.15), because it is in the second stage and this sample in particular reveals the maximum increase of GMR per unit of x, as can be seen in figure 4.1; in fact also the trend of GMR vs $(M/M_{sat})^2$ (figure 4.7) confirms that this sample is the best arrangement between the Fe dilution in Ag and the Fe grain dimension. The hyperfine parameter obtained by best fitting one reported in Tab.4.1. The value of isomeric shift of the singlet (0.50 ± 0.05 mm/s) confirms the hypothesis that is due to dilute impurities of Fe in Ag host, in agreement with the value given by Wagner [46]. The isomer shift of the first quadrupole splitting (D1) is very similar to Fe bulk. The value of quadrupole splitting indicates that the Fe atoms are arranged in a cubical grid considerably deformed. For this, it was attributed to atoms within the cluster of Fe. The value of the isomeric shift of the second quadrupole splitting (D2) suggests that it is ascribable to Fe atoms located at the surface of the clusters [47].

4.5 Study of the system at low temperatures and low magnetic field

Field-cooled (FC) and zero-field-cooled (ZFC) magnetization experiments at low field are very useful for evidencing superparamagnetic properties. During the ZFC the sample is cooled without applied field from room temperature (Fe particles are in a superparamagnetic state at room temperature) down to the lowest temperature T_{min}. Afterward, a low field is applied and the measurement is performed with increasing the temperature. If the magnetization in the superparamagnetic state has to be studied, the above condition on the initial temperature must be fulfilled. For FC measurement the process is the same as for ZFC experiments except that the cooling is done under H_{app} but here the condition related to the superparamagnetic state at the initial temperature is very important. If an appreciable population of the largest particles is blocked at the initial temperature because their magnetic relaxation times are still slow, the initial magnetic state of the samples is not well known, due to the fact that the magnetic state of the blocked particles depends on the thermal history of the sample. This alters the M_{FC} values by an unknown part that can vary with temperature and yields uncertain quantitative estimation. Magnetization M_{FC} always follows the same variation of ZFC. On decreasing the temperature, M_{FC} is merged with M_{ZFC} until T_{irr}, then M_{FC} continues to increase and from a certain temperature T_{sat}, M_{FC} remains constant. On increasing the temperature, magnetization M_{ZFC} increases and shows a maximum for a temperature T_{max}, related to T_B, afterward M_{ZFC} decreases. In absence of an energy barrier (volume) distribution, the three temperatures T_{irr}, T_{max} and T_{sat} are very close to each other (see fig. 4.16a).

FC and ZFC data were collected for different samples and they suggest that, as a function of x, the system goes through different magnetic regimes

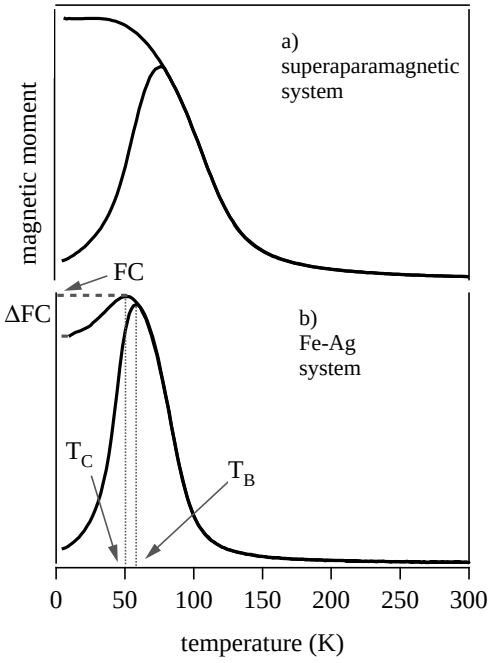

Figure 4.16: In the figure a) there is the shape of a typical FC-ZFC measurement for a superparamagnetic sample; in figure b) the trend observed in a few Fe-Ag samples is presented.

(see figure 4.17): in the low concentration regime the ZFC curves show a well defined, narrow peak, centred at $T = T_B$ typical of disordered system (e.g. spin glass system) [48, 49]. The FC curves display an unexpected maximum at the same temperature and for lower temperatures the FC signal decreases. The irreversibility starts at T_B, not above it. In the intermediate concentration regime, the ZFC curves show a well defined peak centred at $T = T_B$ and the FC magnetization increases monotonically as temperature decreases, a behaviour typical of superparamagnetic systems. The irreversibility starts at $T_{irr} = T_B$. In the high concentration regime, the ZFC curve does not display a well defined peak and the FC curve increases monotonically as temperature decreases. Samples behaviour does not resemble the standard superparamagnetic one.

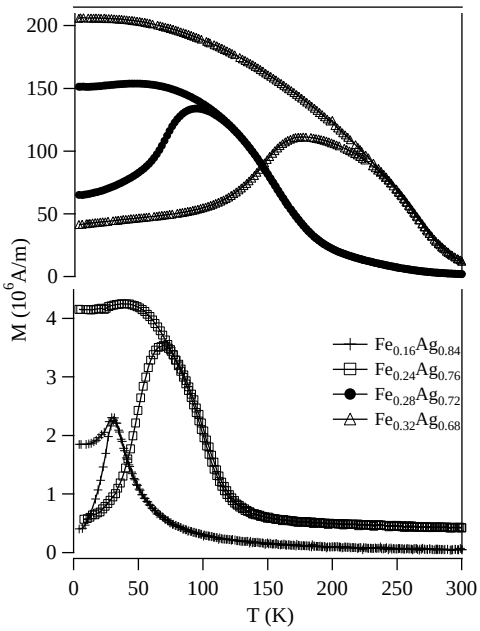

Figure 4.17: The trend of FC-ZFC for different atomic Fe concentration.

The anomaly of FC is the counterpart of a phenomenon that is opposed to the magnetic order of the system given from the external applied field. The dipolar interactions are weak in this range concentration because they are proportional to the volume of the clusters, so it is likely that RKKY (Ruderman, Kittel, Kasuya, Yosida) interactions carried by the mixed matrix are the reason of the anomaly. It is possible to define a few parameters to study the FC anomalies, as can be seen in figure 4.16b. T_C is the temperature where the FC signal starts to decrease; FC is the maximum magnetic moment value of the FC signal and ΔFC is the different between the FC and the magnetic moment value at 4 K, so $\Delta FC/FC$ is the relative decrease of the FC signal. These parameters, together with the trend of T_B, were reported in figure 4.18, as a function of atomic Fe concentration. Considering the trend of $\Delta FC/FC$ vs x, it is possible to distinguish two regions: the first, for $x < 0.20$, where the FC anomaly increase with x and T_B and T_C have the same trend as a function of x. In this region the FC magnetization

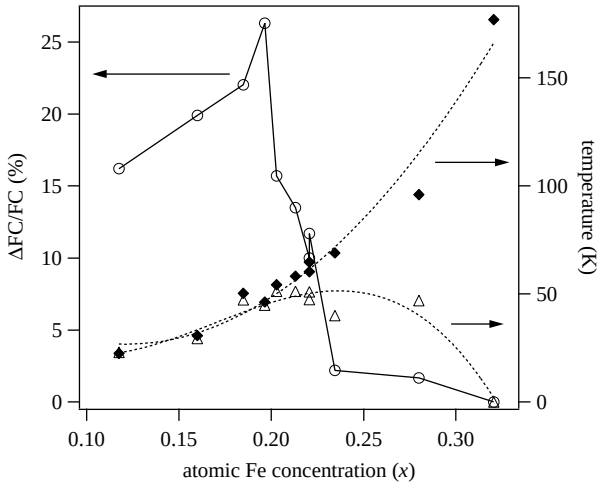

Figure 4.18: The trend of $\Delta FC/FC$ (left axis), T_B and T_C (right axis) as a function of x.

does not keep increasing below T_B, as it occurs in superparamagnets, but decreases, as it was reported in spin-glasses particle systems. The origin of such interparticle interaction may be RKKY that operate through the matrix of Fe-Ag solid solution producing a collective spin glass phase below T_B. In the second region, for $0.20 < x < 0.32$, the effect decrease as a function of x until $x = 0.32$ where it disappears. A dipolar interaction between Fe cluster may set in, mitigating the frustrated magnetic state. In fact, with increasing x, there is the presence of a wide distribution of cluster size in the system, so the dipolar effect of interactions is enhanced.

Besides, the particles average size obtained from T_B [15] is larger than the value calculated from room temperature magnetization and magnetoresistance data; interactions produce a magnetic coalescence of the particles. In particular, the overall size, proportional to T_B, increases with x.

ΔFC/FC exponentially decreases as a function of the external field intensity, H, used during the cooling procedure: ΔFC/FC $\sim$ exp(-H/H_0) (see figure 4.19). The trend of H_0 as a function of x is presented in figure 4.20.

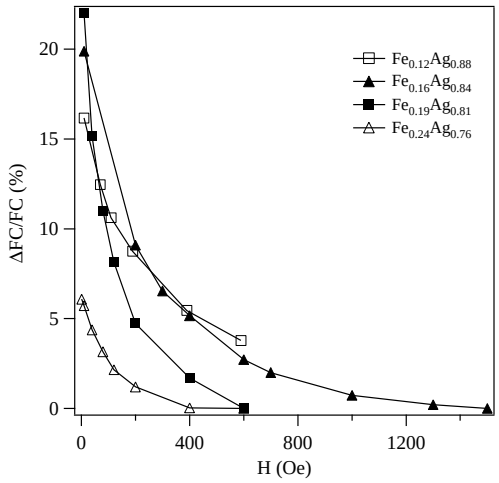

Figure 4.19: The trend of $\Delta FC/FC$ as a function of magnetic field for different samples.

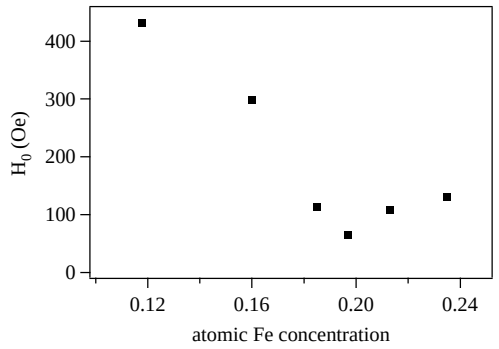

Figure 4.20: The trend of H_0 as a function of x.

The $H_0(x)$ behaviour can be explained in this way: starting from $x = 0.12$, as more Fe is introduced the disordered magnetic regions get wider, frustrated interactions get stronger and propagate on a larger scale, thus involving larger samples volumes. Due to this effect H_0 decreases. For $x > 0.20$ a regime ruled by dipolar interactions sets in and the frustrated magnetic regions are reduced in size, so H_0 shows a slight increase as a condition similar to that found in the low concentration regime is restored.

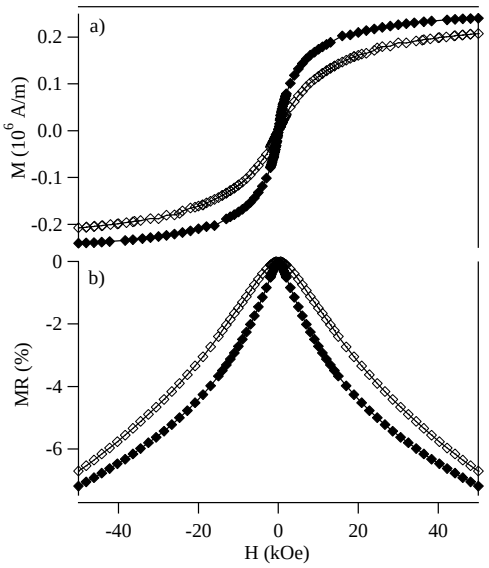

Figure 4.21: The comparison between the MvsH (a) and MRvsH (b) curves for the sample $Fe_{0.24}Ag_{0.76}$ before (◊) and after (⧫) the thermal treatment.

4.6 Thermal treatment

To comprehend what is the best structural arrangement of Fe in Ag to have the maximum of GMR it is necessary understand if the increase of GMR depends on the increase of the number of clusters of Fe or by increasing their volume and confirm the hypothesis on the magnetic interactions between magnetic clusters. For these reasons selected samples were submitted to a heat treatment at 200°C for 2 h in Ar atmosphere, carried out by using a Differential Scanning Calorimeter. It is known that thermal annealing promotes the clustering of Fe atoms originally dispersed in Ag matrix.

The GMR effect increase with the thermal treatment in the second regime that is for $0.2 < x < 0.32$. For lower concentration there is a little increase of GMR with the treatment instead for higher concentration, where is the maximum GMR effect, the intensity of GMR effect at 1.3 T is constant (see figure 4.21b). Also the magnetization data of the sample before and after

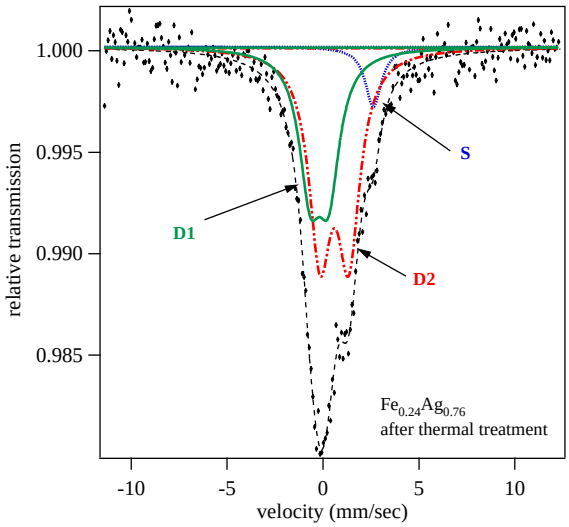

Figure 4.22: Mössbauer data (solid symbols) and fit (dotted line) for the $Fe_{0.24}Ag_{0.76}$ as after thermal treatment. Straight lines represent the three contributions used to fit the data to the model presented in the text.

the thermal treatment are different: after the treatment the magnetization at 5 T is larger and the response at the magnetic field is quicker (fig. 4.21a)

Contribution	Is (mm/s)	Qs (mm/s)	Fe rate
singlet (S)	0.65 ± 0.03	/	6%
doublet one (D1)	-0.05 ± 0.02	5.23 ± 0.86	37%
doublet two (D2)	0.15 ± 0.01	8.08 ± 0.29	57%

Table 4.2: Isomeric shift (IS) and quadrupole splitting (QS) of fit of Mössbauer spectra for the sample $Fe_{0.24}Ag_{0.76}$ after the thermal treatment

The Mössbauer investigation was made on samples after the thermal treatment, as well, to understand how the structure of the samples changes with the thermal treatment. The Mössbauer spectra after the thermal treatment for the sample $Fe_{0.24}Ag_{0.76}$ are related in figure 4.22 and the fit parameters are reported in Tab.4.2. The heat treatment reduces the percentage

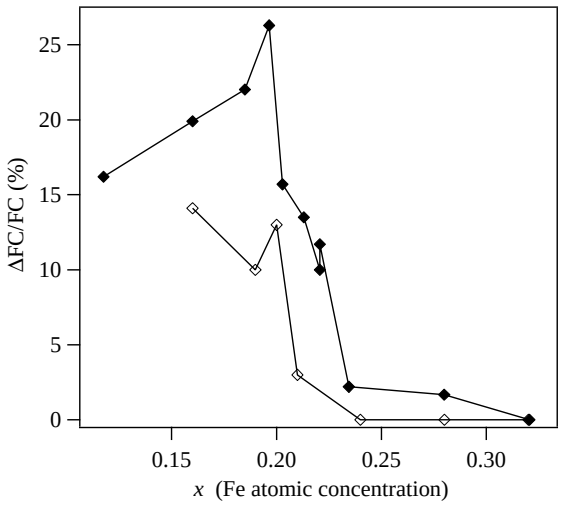

Figure 4.23: The trend of $\Delta FC/FC$ as a function of x before (⧫) and after (◊) the thermal treatment.

of the total resonant absorption of the singlet and increases the percentage of the doublet D2. The quadrupole splitting value of two doublets does not change, within the experimental error. So the thermal treatment does not affect the distortion of the crystal lattice. Furthermore, the fact that the shift of both the doublets does not change significantly, indicates that the composition of cluster is not affected by the heat treatment. Furthermore if we analyze the trend of MR in function of H, for H up to 5 T, we note that for $x < 0.2$ the curve shape is the same before and after the thermal treatment, instead for $0.2 < x < 0.32$ the GMR is more rapid for low H but for high H the trend is the same. This confirms that the thermal treatment for $0.2 < x < 0.32$ increases the number of clusters without significatively affecting their size while for $x > 0.32$ the treatment increases above all the size of the cluster within the system, so the GMR does not increase. So the Mössbauer results with the magnetoresistance data for the samples after the thermal treatment confirm that GMR increase depends on the increase of the number of Fe clusters.

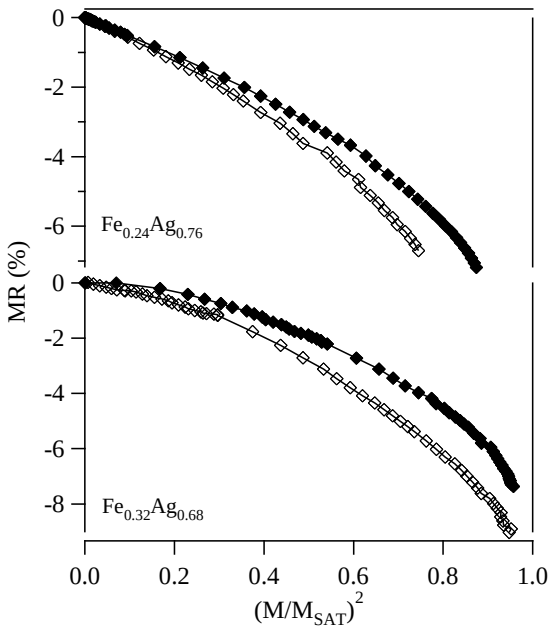

Figure 4.24: The trend of MR vs M/M_{sat}^2 for the samples $Fe_{0.24}Ag_{0.76}$ and $Fe_{0.32}Ag_{0.68}$ before ($\Diamond$) and after ($\blacklozenge$) the thermal treatment.

The thermal treatment should reduce the anomaly of the FC signal because if the anomaly is imputable to the magnetic interactions carried by the mixed Fe-Ag disordered phase, the thermal treatment reduces amount of Fe dispersed in the Ag matrix so it reduces the magnetic interactions, too. As ΔFC is reduced by thermal annealing (see figure 4.23), so this confirms that FC signal anomaly may be ascribed to the presence of the disordered magnetic phase. Indeed, as the equilibrium Fe-Ag miscibility is zero, due to the thermal treatment Fe precipitates are produced and Fe atoms are removed from the solid solution; this reduces the influence of the mixed Fe-Ag disordered phase. The trend of GMR vs $(M/M_{sat})^2$ after the thermal treatment for two samples with different Fe concentration is presented in figure 4.24. The differences from the linear expected behaviour increase after the thermal treatment, particularly for high values of the magnetic field for the samples with lower x, instead for higher Fe concentration the trend is different for

all field values. The thermal treatment promotes the clustering of Fe atoms, then the MR efficiency decreases because the number of small size clusters decreases and the magnetic interactions between Fe clusters become more effective. The results indicate that, for the studied samples, the distribution of magnetic moments may explain the noncompliance with the square law of the magnetoresistance as a function of the magnetization as expected for an assembly of equal superparamagnetic particles.

4.7 Correlation between magnetic and structural measurements

In the low atomic Fe concentration regime ($x < 0.20$), diffraction measurements point out that the structure of the samples is a not-saturated solid solution of Fe-Ag with Fe atoms that occupy sostitutional position in the Ag lattice (fcc) and small Fe precipitates which presence is confirmed by the superparamagnetic signal observed at room temperature. The low temperature and low field magnetic measurements suggest that there is a decrease of FC signal that is possibly ascribable to a frustrated magnetic behaviour. Therefore the sample maybe behaves like a cluster glass system, where RKKY interactions acting through the mixed Fe-Ag matrix give rise to the observed frustrated behaviour.

For intermediate concentration regime ($0.20 < x < 0.27$) the lattice dependence on x changes with respect to the previous regime, indicating that there is not only a Fe-Ag solid solution but also large Fe precipitates start growing within the sample. The magnetic measurements (FC/ZFC) indicate that the relative reduction of FC magnetization decreases, so it is possible that a different kind of interparticle interaction, like dipolar ones, competes with the glassy behaviour.

For the high concentration regime ($x > 0.27$) diffraction spectra dis-

play new reflections possibly ascribable to a BCC iron phase and the shape of FC/ZFC curves strongly deviates from the clear superparamagnetic behaviour and indicates that strong magnetic interactions act on the system. At this concentration are present both contact interactions between the Fe clusters, because they have notable size and non contact interactions, like dipolar and RKKY interactions, between the small particles. Both elements support the hypothesis that competing interactions among magnetic moments result in a frustrated ferromagnetic state [34].

Chapter 5

Conclusions

The giant magnetoresistive effect was investigated in Fe_xAg_{1-x} nanogranular films grown with *dc* magnetron co-sputtering. Increasing the atomic Fe concentration, both the GMR effect and the GMR efficiency increase. The maximum of efficiency has been observed for $x = 0.26$, while the maximum of effect appears for $x = 0.32$. The structural investigation reveals that at low Fe concentration there is a Fe-Ag not-saturated solid solution together the presence of small Fe aggregates, that are detected from magnetic measurements. Increasing x the size of Fe aggregates, embedded in the non-satured solid solution, increases. For high Fe concentration, $x > 0.32$, the solid solution is saturated and the new bcc-Fe phase rises. At these concentrations the Fe clusters are at the percolation theresold [39]. The magnetic investigation at low field and low temperature reveals, for $x < 0.32$, the presence of two regimes. The first, for low x, is a collective spin glass phase that indicate a frustration of the system for $T < T_B$, where there are interparticle interactions, maybe RKKY, that operate through the matrix, namely the Fe-Ag non-satured solid solution. In confirmation of this, the thermal treatment, that promotes the clustering of Fe atoms originally dispersed in Ag matrix, hampers the frustrated behaviour. The second, increasing x, where the dipolar interactions between Fe clusters set in and mitigate the frustrated

magnetic state. Above $x = 0.32$ the system has not a superparamagnetic behaviour but it is a frustrated ferromagnet.

At the concentration of the GMR maximum ($x = 0.32$) the structural investigations reveal the presence of a saturated solid solution of Fe-Ag and Fe BCC clusters. The magnetic measurements highlight the presence of Fe nanoclusters with an average size that is comparable with that of nanocrystals of the Fe-Ag solid solution and reveal the presence of strong magnetic interaction among the Fe clusters. At this concentration, the frustrated magnetic behaviour disappears, as well.

At the concentration of the maximum GMR efficiency ($x = 0.26$) the structural investigations reveal that there are Fe clusters with average size of some nanometres, embedded in a non-satured solid solution and the magnetic investigations disclose the presence of dipolar magnetic interactions that attenuate the magnetic frustation observed for lower concentration.

In this case the maximum GMR effect is the best arrangement between a structure that displays the maximum efficiency and a structure with a raised concentration of scattering centres, that is a raised magnetic material concentration. The maximum effect is detected when the sample is formed of a big number of cluster with dimension around a few nanometres and a disordered matrix including very fine Fe clusters. Both the Fe cluster and the little aggregates dispersed in the matrix participate in the GMR effect because there is a big volume/surface ratio that increase the GMR effect and decrease the dipolar interactions. In summary to have the maximum effect, the raised amount of magnetic material present in the system has a best arrangement (like at the concentration of the maximum GMR efficiency) in the non-magnetic matrix, and the distance between the magnetic aggregates is of the order of the conduction electrons mean free path.

Bibliography

[1] G. Binasch, P. Grünberg, F. Saurenbach, and W. Zinn, Phys. Rev. B **39**, 4828 (1989).

[2] M. N. Baibich *et al.*, Phys. Rev. Lett. **61**, 2472 (1988).

[3] S. S. Parkin, A. Modak, and D. J. Smith, Phys. Rev. B **47**, 9136 (1993).

[4] J. Barnas *et al.*, Phys. Rev. B **42**, 8110 (1990).

[5] N. F. Mott, Proc. Royal Soc. **156**, 368 (1936).

[6] N. F. Mott, Adv. Phys. **13**, 325 (1964).

[7] P. Schroeder *et al.*, *Interfaces and Characterization. Materials Research Society Symposium Proceedings* (MRS, Pittsburg, PA, 1993), Vol. 313, p. 47.

[8] N. Ashcroft and N. Mermin, *Solis State Physics* (Saunders College, Philadelphia, 1976).

[9] T. Valet and A. Fert, Phys. Rev. B **48**, 7099 (1993).

[10] M. Johnson and R. H. Silsbee, Phys. Rev. Lett. **55**, 1790 (1985).

[11] A. E. Berkowitz *et al.*, Phys. Rev. Lett. **68**, 3745 (1992).

[12] J. Q. Xiao, J. Jiang, and C. L. Chien, Phys. Rev. Lett. **68**, 3749 (1992).

[13] J. Q. Wang and G. Xiao, Phys. Rev. B **49**, 3982 (1994).

[14] C. Kittel, Phys. Rev. **70**, 965 (1946).

[15] J. Dormann, D. Fiorani, and E. Tronc, *Advances in Chemical Physics* (John Wiley and Sons, Inc., 1997), Vol. XCVIII, p. 283.

[16] E. Stoner and E. Wohlfarth, Philos. Trans. R. Soc. London, Ser.A **240**, 599 (1948).

[17] C. Binns *et al.*, Phys. Rev. B **66**, 184413 (2002).

[18] P. Allia *et al.*, Phys. Rev. B **60**, 12207 (1999).

[19] P. Allia, K. Knobel, P. Tiberto, and F. Vinai, Phys. Rev. B **52**, 15398 (1995).

[20] E. F. Ferrari, F. C. S. da Silva, and M. Knobel, Phys. Rev. B **56**, 6086 (1997).

[21] B. J. Hickey, M. A. Howson, S. O. Musa, and N. Wiser, Phys. Rev. B **51**, 667 (1995).

[22] J. F. Gregg *et al.*, Phys. Rev. B **49**, 1064 (1994).

[23] S. Zhang and P. M. Levy, J. Appl. Phys. **73**, 5315 (1993).

[24] Y. Asano, A. Oguri, J. Inoue, and S. Maekawa, Phys. Rev. B **49**, 12831 (1994).

[25] D. Kechrakos and N. Trohidou, Phys. Rev. B **62**, 3941 (2000).

[26] O. Kappertz, R. Drese, and M. Wuttig, J. Vac. Sci. Technol. A **20**, 2084 (2002).

[27] R. Wendt and K. Ellmer, Surface and Coatings Technology **93**, 27 (1997).

[28] R. Wendt, K. Ellmer, and K. Wiesemann, J. Appl. Phys. **82**, 2115 (1997).

[29] M. Hansen, *Constitution of binary alloys* (McGraw-Hill book co, New York, 1958).

[30] M. Baricco, private communication.

[31] G. Xiao, J. Q. Wang, and P. Xiong, Appl. Phys. Lett. **62**, 420 (1993).

[32] F. Casoli *et al.*, Scripta Materialia **48**, 955 (2003).

[33] D. Kechrakos and N. Trohidou, J. Appl. Phys. **89**, 7293 (2001).

[34] P. Allia *et al.*, Phys. Rev. B **73**, 054409 (2006).

[35] N. Kataoka, K. Sumiyama, and Y. Nakamura, J. Phys. F: Met. Phys. **15**, 1405 (1985).

[36] A. L. Patterson, Phys. Rev. **56**, 978 (1939).

[37] H. Wan, A. Tsoukatos, and G. C. Hadjipanayis, Phys. Rev. B **49**, 1524 (1994).

[38] A. R. Denton and N. W. Ashcroft, Phys. Rev. A **43**, 3161 (1991).

[39] D. Bisero *et al.*, J. Magn. Magn. Mater. **262**, 84 (2003).

[40] Y. Xu *et al.*, J. Appl. Phys. **76**, 2969 (1994).

[41] N. Kataoka, K. Sumiyama, and Y. Nakamura, J. Phys. F: Met. Phys. **18**, 1049 (1988).

[42] G. Xiao *et al.*, Phys. Rev. B **34**, 7573 (1986).

[43] M. K. Roy, P. Nambissan, and H. Verma, J. Alloys Com. **345**, 183 (2002).

[44] J. Q. Wang and G. Xiao, Phys. Rev. B **51**, 5863 (1995).

[45] F. Spizzo *et al.*, J. Magn. Magn. Mater. **272**, 1169 (2004).

[46] G. K. Shenoy and F. Wagner, *Mossbauer Isomer Shift* (North-Holland, Amsterdam, 1978).

[47] G. Rixecker, Sol. State Commun. **122**, 299 (2002).

[48] K. H. Fischer, Phys. Stat. Sol. B **116**, 357 (1983).

[49] K. Binder and A. P. Young, Rev. Mod. Phys. **58**, 801 (1986).

Acknowledgment

Prima di tutto vorrei ringraziare il mio tutore, prof. Franco Ronconi, per la disponibilità che mi ha concesso in questi anni ma soprattutto per l'insegnamento elargitomi.

Un grazie infinitamente grande al dott. Federico Spizzo perchè nonostante i molteplici impegni mi ha dedicato tutto il tempo che gli era possibile e anche di più, mi ha consigliato e aiutato in ogni momento in cui avessi bisogno.

Grazie al prof. Michele Sacerdoti del Dipartimento di Scienze della Terra dell'Università degli Studi di Ferrara e al prof. Giancarlo Battaglin del Dipartimento di Chimica Fisica dell'Università Ca' Foscari di Venezia per la disponibilit dimostrata e le competenze che mi hanno elargito.

Grazie a Massimo, per la sua pazienza, la sua disponibilità, e ora come non mai per la sua presenza nella mia vita.